

Search for Nucleon Decay into Charged Anti-lepton plus Meson in Super-Kamiokande I and II

H. Nishino,^{2,*} K. Abe,¹ Y. Hayato,^{1,27} T. Iida,¹ M. Ikeda,¹ J. Kameda,¹ Y. Koshio,¹ M. Miura,¹ S. Moriyama,^{1,27} M. Nakahata,^{1,27} S. Nakayama,¹ Y. Obayashi,¹ H. Sekiya,¹ M. Shiozawa,^{1,27} Y. Suzuki,^{1,27} A. Takeda,¹ Y. Takenaga,¹ Y. Takeuchi,^{1,27} K. Ueno,¹ K. Ueshima,¹ H. Watanabe,¹ S. Yamada,¹ S. Hazama,² I. Higuchi,² C. Ishihara,² H. Kaji,² T. Kajita,^{2,27} K. Kaneyuki,^{2,27,†} G. Mitsuka,² K. Okumura,² N. Tanimoto,² F. Dufour,³ E. Kearns,^{3,27} M. Litos,³ J. L. Raaf,³ J. L. Stone,^{3,27} L. R. Sulak,³ M. Goldhaber,^{4,†} K. Bays,⁵ J. P. Cravens,⁵ W. R. Kropp,⁵ S. Mine,⁵ C. Regis,⁵ M. B. Smy,^{5,27} H. W. Sobel,^{5,27} K. S. Ganezer,⁶ J. Hill,⁶ W. E. Keig,⁶ J. S. Jang,⁷ J. Y. Kim,⁷ I. T. Lim,⁷ J. B. Albert,⁸ K. Scholberg,^{8,27} C. W. Walter,^{8,27} R. Wendell,⁸ T. Ishizuka,⁹ S. Tasaka,¹⁰ J. G. Learned,¹¹ S. Matsuno,¹¹ Y. Watanabe,¹² T. Hasegawa,¹³ T. Ishida,¹³ T. Ishii,¹³ T. Kobayashi,¹³ T. Nakadaira,¹³ K. Nakamura,^{13,27} K. Nishikawa,¹³ Y. Oyama,¹³ K. Sakashita,¹³ T. Sekiguchi,¹³ T. Tsukamoto,¹³ A. T. Suzuki,¹⁴ A. Minamino,¹⁵ T. Nakaya,^{15,27} M. Yokoyama,¹⁵ Y. Fukuda,¹⁶ Y. Itow,¹⁷ T. Tanaka,¹⁷ C. K. Jung,¹⁸ G. Lopez,¹⁸ C. McGrew,¹⁸ C. Yanagisawa,¹⁸ N. Tamura,¹⁹ Y. Idehara,²⁰ M. Sakuda,²⁰ Y. Kuno,²¹ M. Yoshida,²¹ S. B. Kim,²² B. S. Yang,²² H. Okazawa,²³ Y. Choi,²⁴ H. K. Seo,²⁴ Y. Furuse,²⁵ K. Nishijima,²⁵ Y. Yokosawa,²⁵ M. Koshihara,²⁶ Y. Totsuka,^{26,†} M. R. Vagins,^{27,5} S. Chen,²⁸ Y. Heng,²⁸ J. Liu,²⁸ Z. Yang,²⁸ H. Zhang,²⁸ D. Kielczewska,²⁹ K. Connolly,³⁰ E. Thrane,³⁰ and R. J. Wilkes³⁰

(The Super-Kamiokande Collaboration)

¹*Kamioka Observatory, Institute for Cosmic Ray Research, University of Tokyo, Kamioka, Gifu 506-1205, Japan*

²*Research Center for Cosmic Neutrinos, Institute for Cosmic Ray Research, University of Tokyo, Kashiwa, Chiba 277-8582, Japan*

³*Department of Physics, Boston University, Boston, MA 02215, USA*

⁴*Physics Department, Brookhaven National Laboratory, Upton, NY 11973, USA*

⁵*Department of Physics and Astronomy, University of California, Irvine, Irvine, CA 92697-4575, USA*

⁶*Department of Physics, California State University, Dominguez Hills, Carson, CA 90747, USA*

⁷*Department of Physics, Chonnam National University, Kwangju 500-757, Korea*

⁸*Department of Physics, Duke University, Durham NC 27708, USA*

⁹*Junior College, Fukuoka Institute of Technology, Fukuoka, Fukuoka 811-0295, Japan*

¹⁰*Department of Physics, Gifu University, Gifu, Gifu 501-1193, Japan*

¹¹*Department of Physics and Astronomy, University of Hawaii, Honolulu, HI 96822, USA*

¹²*Physics Division, Department of Engineering, Kanagawa University, Kanagawa, Yokohama 221-8686, Japan*

¹³*High Energy Accelerator Research Organization (KEK), Tsukuba, Ibaraki 305-0801, Japan*

¹⁴*Department of Physics, Kobe University, Kobe, Hyogo 657-8501, Japan*

¹⁵*Department of Physics, Kyoto University, Kyoto, Kyoto 606-8502, Japan*

¹⁶*Department of Physics, Miyagi University of Education, Sendai, Miyagi 980-0845, Japan*

¹⁷*Solar Terrestrial Environment Laboratory, Nagoya University, Nagoya, Aichi 464-8602, Japan*

¹⁸*Department of Physics and Astronomy, State University of New York, Stony Brook, NY 11794-3800, USA*

¹⁹*Department of Physics, Niigata University, Niigata, Niigata 950-2181, Japan*

²⁰*Department of Physics, Okayama University, Okayama, Okayama 700-8530, Japan*

²¹*Department of Physics, Osaka University, Toyonaka, Osaka 560-0043, Japan*

²²*Department of Physics, Seoul National University, Seoul 151-742, Korea*

²³*Department of Informatics in Social Welfare, Shizuoka University of Welfare, Yaizu, Shizuoka, 425-8611, Japan*

²⁴*Department of Physics, Sungkyunkwan University, Suwon 440-746, Korea*

²⁵*Department of Physics, Tokai University, Hiratsuka, Kanagawa 259-1292, Japan*

²⁶*The University of Tokyo, Bunkyo, Tokyo 113-0033, Japan*

²⁷*Institute for the Physics and Mathematics of the Universe, Todai Institutes*

for Advanced Study, University of Tokyo, Kashiwa, Chiba 277-8582, Japan

²⁸*Department of Engineering Physics, Tsinghua University, Beijing, 100084, China*

²⁹*Institute of Experimental Physics, Warsaw University, 00-681 Warsaw, Poland*

³⁰*Department of Physics, University of Washington, Seattle, WA 98195-1560, USA*

(Dated: November 23, 2018)

Searches for a nucleon decay into a charged anti-lepton (e^+ or μ^+) plus a light meson (π^0 , π^- , η , ρ^0 , ρ^- , ω) were performed using the Super-Kamiokande I and II data. Twelve nucleon decay modes were searched for. The total exposure is 140.9 kiloton-years, which includes a 91.7 kiloton-year exposure (1489.2 live days) of Super-Kamiokande-I and a 49.2 kiloton-year exposure (798.6 live days) of Super-Kamiokande-II. The number of candidate events in the data was consistent with the atmospheric neutrino background expectation. No significant evidence for a nucleon decay was observed in the data. Thus, lower limits on the nucleon partial lifetime at 90% confidence level were obtained. The limits range from 3.6×10^{31} to 8.2×10^{33} years, depending on the decay modes.

I. INTRODUCTION

The standard model of particle physics has been successful in explaining most experimental results. However, it contains many empirical parameters, such as masses and generations of fermions, coupling constants, mixing angles, and so on. Grand Unified Theories (GUTs) have been proposed to account for these parameters. The basic idea of GUTs is that the $SU(2) \times U(1)$ symmetry of electroweak interactions and the $SU(3)$ color symmetry of strong interactions are incorporated into a larger symmetry group broken at an ultra-high energy scale. GUTs predict new interactions in which leptons and quarks can transform one into the other by exchanging a super-heavy gauge boson. This type of interaction can lead to baryon number violating nucleon decays. The simplest GUT, minimal $SU(5)$ [1], predicts the partial lifetime of a proton via the mode $p \rightarrow e^+ \pi^0$ to be $\sim 10^{31 \pm 1}$ years [2, 3], which was excluded by the IMB and KAMIOKANDE experiments [4, 5].

There are various viable GUTs (see, e.g., [6–12]), such as models incorporating supersymmetry (SUSY), models with a symmetry group like $SO(10)$, flipped $SU(5)$ models, and models in extra dimensions. Predictions for the lifetime of the nucleon strongly depend on the models and also have large uncertainties. Some models predict the partial lifetime of the proton to be in the accessible range of the Super-Kamiokande experiment.

The Super-Kamiokande collaboration previously published the results of $p \rightarrow e^+ \pi^0$ and $p \rightarrow \mu^+ \pi^0$ searches [13]. Updated results have also been presented since that time [14]. No candidate events for proton decay were found. Although the $p \rightarrow e^+ \pi^0$ mode is considered to be the dominant decay mode in many GUT models, branching ratios for the other modes are not necessarily negligible. Many possibilities for nucleon decays are theoretically proposed. In some $SU(5)$ and $SO(10)$ GUT models ([15–18]), branching ratios for $p \rightarrow e^+ \eta$, $p \rightarrow e^+ \rho^0$ or $p \rightarrow e^+ \omega$ can be as high as $10 \sim 20\%$ and the proton and bound neutron lifetimes are expected to be comparable to each other. Also, $N \rightarrow \mu^+ + meson$ modes can be induced by mixing effects between lepton families. Though typical $SU(5)$ GUT models predict very small branching ratios for the muon modes (see, e.g., [15, 19]), the flipped $SU(5)$ GUT [12] shows that the $p \rightarrow \mu^+ \pi^0$ mode can have a comparable branching ratio with the $p \rightarrow e^+ \pi^0$ mode. Therefore, nucleon decay modes mediated by the exchange of super-heavy gauge bosons are important for most of the GUT models. In spite of the importance of investigating all possible decay modes, so

far only the $p \rightarrow e^+ \pi^0$ and $p \rightarrow \mu^+ \pi^0$ searches, and the searches for several modes favored by SUSY GUTs [20] have been published by the Super-Kamiokande experiment. In this paper, we search for nucleon decays into a charged anti-lepton (e^+ and μ^+) plus an un-flavored light meson (π , η , ρ and ω) using the Super-Kamiokande I and II data. Eight modes were studied for proton decay, and four for neutron decay. The results of the $p \rightarrow e^+ \pi^0$ and $p \rightarrow \mu^+ \pi^0$ mode are identical to those reported in an earlier Letter [13], however more details of the analysis are described in this paper. In addition, we briefly report the results of the search in these two channels based on a longer exposure including Super-Kamiokande III and IV data.

II. SUPER-KAMIOKANDE DETECTOR

Super-Kamiokande is a 50-kiloton water Cherenkov detector located in the Kamioka Observatory in Japan, under ~ 1000 m of rock overburden. The Super-Kamiokande detector is made of a cylindrical stainless steel tank, 39.3 m in diameter and 41.4 m in height. The detector is optically separated into two regions: an inner detector (ID), and an outer detector (OD). On the surface of the ID, 20-inch photomultiplier tubes (PMTs) are uniformly attached to detect Cherenkov light radiated by relativistic charged particles. The OD, which surrounds the ID with a 2 m thickness of water, is used to reject cosmic ray muon events and to tag exiting charged particles with 1,885 outward-facing 8-inch PMTs. The OD region also serves as a shield from radioactivity from materials outside the detector wall.

The Super-Kamiokande experiment started data-taking in April, 1996, and had continued observation for five years until the detector maintenance in July 2001 (SK-I). On November 2001, while filling the tank with water after the maintenance, an accident occurred which destroyed more than half of the PMTs. The detector was partially rebuilt with half the density of photo-sensor coverage in the ID. Observation began again in October 2002 and stopped in October 2005 (SK-II) for a full detector reconstruction. The next phase, SK-III, started October 2006 and was switched to SK-IV with newly developed electronics and online systems in September 2008. This paper reports nucleon decay search results from the first two periods: SK-I and SK-II. The ID photo-sensor coverage in the SK-I period was 40% with 11,146 20-inch PMTs. In the SK-II period, the coverage reduced to 19% with 5,182 20-inch PMTs. All of the ID PMTs have been equipped with acrylic covers and fiber-reinforced plastic cases since the start of SK-II to avoid a cascade of implosions of PMTs. Details of the detector configuration and performance for SK-I have been published [21].

* Present address: University of California, Berkeley, CA 94720, USA

† Deceased.

III. SIMULATION

A. Nucleon Decay Simulation

In order to estimate the detection efficiencies of nucleon decays, a nucleon decay Monte Carlo (MC) simulation was developed. The number of background events was estimated by simulations of the atmospheric neutrino flux and neutrino interactions.

In an H₂O molecule, there are two free protons in the hydrogen nuclei, and eight bound protons and eight bound neutrons in the oxygen nucleus. The decay probabilities of free protons and bound protons were assumed to be equal in the simulation. All of the decay modes studied in this analysis are two-body decays, meaning that the charged lepton and meson are back-to-back with a monochromatic momentum in the nucleon rest frame.

For the decay of bound nucleons in oxygen, the simulation takes into account the effect of Fermi motion of the nucleons, correlation with another nucleon, and meson-nucleon interactions in the nucleus (nuclear effects). Nucleon momentum and nuclear binding energy in the nucleus were calculated as described in [22]. Good agreement of the calculations with an electron scattering experiment on ¹²C is also shown in [22].

Mesons generated in an oxygen nucleus interact with nucleons until they escape from the nucleus. The position of the nucleon decay in a nucleus was determined by the Woods-Saxon nuclear density distribution in the simulation. From this position, π , η and ω mesons were tracked in an oxygen nucleus. The lifetime of the ρ meson is so short ($\beta\gamma\tau \simeq 0.3$ fm) that it decays immediately inside the nucleus into 2 π mesons; therefore, the nuclear effects of the ρ meson itself were not considered in the simulation. The mass of the ρ meson was assumed to have a Breit-Wigner type distribution with a width of $\Gamma = 149$ MeV. For these reasons, particles generated via the modes including a ρ meson do not have monochromatic momentum, even in the case of free proton decay.

Ten percent of nucleons in oxygen were assumed to decay correlating with another nucleon [23]. In such correlated decay events, the invariant mass of e^+ and π^0 is smaller than the mass of the nucleon because of the invisible momentum of another correlated nucleon.

Simulated particles of nucleon decays and atmospheric neutrino interactions were passed through a GEANT-3 [24] custom detector simulation. Hadronic interactions were treated by CALOR [25] for nucleons and charged pions of $p_\pi > 500$ MeV/ c , and by a custom simulation program [26] for charged pions of $p_\pi \leq 500$ MeV/ c .

1. π Meson Nuclear Effects

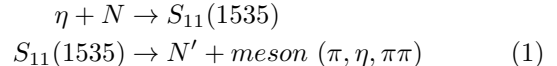
In considering pion nuclear effects, inelastic scattering, absorption, charge exchange and pion production were taken into account in the simulation. Pion production hardly occurs in nucleon decay events since the

cross-section for low momentum pions ($p_\pi < 500$ MeV/ c) is negligibly small. Cross-sections for these processes were calculated based on the model of Oset *et al.* [27]. The angular and momentum distributions of pions were determined from the results of π - N scattering experiments [28]. Because of the Pauli exclusion principle, the momentum of the scattered nucleon is required to be greater than the Fermi surface momentum, given by $p_F(r) = (\frac{3}{2}\pi^2\rho(r))^{\frac{1}{3}}$, where $\rho(r)$ is the nuclear density distribution and r is the distance from the center of the nucleus.

The π^0 momentum from the decay mode of $p \rightarrow e^+\pi^0$ is 459 MeV/ c in the rest frame of the nucleon. At this momentum, 37% of π^0 s were simulated to be absorbed or charged-exchanged in the nucleus. This is a major reason for the inefficiency of the $p \rightarrow e^+\pi^0$ and $p \rightarrow \mu^+\pi^0$ modes. The probability for a π^0 to escape from a nucleus without any scattering was estimated to be 44%.

2. η Meson Nuclear Effect

The interactions of η s and nucleons in the nucleus were considered through a baryon resonance of $S_{11}(1535)$.



The cross-section for η -nucleon interactions shown in Fig. 1 was calculated by the Breit-Wigner formula as follows:

$$\sigma = \frac{\pi}{k^2} \frac{\Gamma_{\eta N} (\Gamma_{\text{total}} - \Gamma_{\eta N})}{(E_{\text{CMS}} - M_{\text{res}})^2 + \Gamma_{\text{total}}^2/4}, \quad (2)$$

where E_{CMS} is the center-of-mass energy of η - N , M_{res} is the mass of the resonance, Γ_{total} is the total width of $S(1535)$ resonance, $\Gamma_{\eta N}$ is the partial width of $S(1535) \rightarrow \eta N$, and k is the wave number (p/\hbar). The net nuclear effect of η -meson in an oxygen nucleus is estimated by using this cross-section as well as considering the nuclear density distribution, nucleon momentum distribution and the Pauli exclusion principle effect in an nucleus. Since pions can be generated by the decay of the resonance, nuclear effects for π mesons were also considered according to Section III A 1. Approximately 56% of η mesons generated by $p \rightarrow e^+\eta$ escaped from the nucleus without any scattering, while 38% of η mesons were absorbed or decayed into other particles from the resonance.

The η meson nuclear effects simulation were checked by a comparison with the experimental cross-section of η photoproduction on a ¹²C target measured at MAINZ [29]. Since photons are insensitive to strong interactions and able to probe the inside of nuclei, meson photoproduction data were used for the study of the nuclear effects. The peak momentum of the η meson in the photoproduction experiment is approximately 300 MeV/ c , which is equivalent to the η momentum generated by $p \rightarrow e^+$ (or μ^+) η . In order to simulate the η

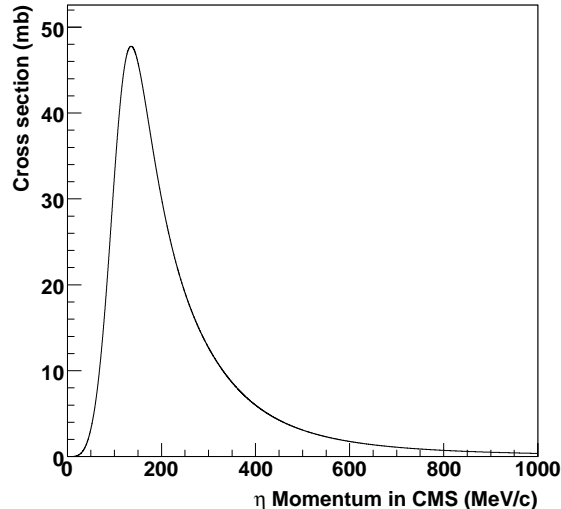


FIG. 1. Calculated cross-section of η -nucleon interaction considering $S_{11}(1535)$ resonance in the custom simulation code.

photoproduction on a ^{12}C target, η mesons were generated following the cross-section data of a proton target from the SAID calculation [30], and tracked in nuclei while suffering the η - N interaction described above. The cross-section on a neutron was assumed to be 2/3 of that of a proton target, since this assumption reproduces the experimental cross-sections of a deuteron target [31].

Figure 2 shows a comparison of the experimental η photoproduction cross-section for a ^{12}C target and the cross-section simulated by our nuclear effects simulation. The simulation predicted well the reduction of the photoproduction cross-section by the nuclear effects. The difference between the experiment and the simulation was taken as the uncertainty of the η nuclear effects. The uncertainty of the cross-section of the η nuclear effects was estimated to be a factor of two.

3. ω Meson Nuclear Effect

The width of the ω meson resonance is $\Gamma = 8.49$ MeV and its lifetime is $\tau = \hbar/\Gamma = 0.77 \times 10^{-22}$ sec. In the proton decay of $p \rightarrow e^+\omega$, the ω meson momentum is ~ 140 MeV/ c so that the mean free path ($\beta\gamma\tau$) of the ω meson is ~ 4 fm. The decay of ω 's was taken into account in the ω meson tracking in the nucleus because the mean free path is comparable to the size of the radius of a nucleus.

The ω meson interactions with a nucleon in an oxygen nucleus were calculated with a boson exchange model by Lykasov *et al.* [32]. The coupling constants and the form factor of this model were fixed by the experimental data. The simulation takes into account reactions such as $\omega N \rightarrow \omega N$, $\omega N \rightarrow \pi N'$, $\omega N \rightarrow \rho N'$, $\omega N \rightarrow \rho\pi N'$,

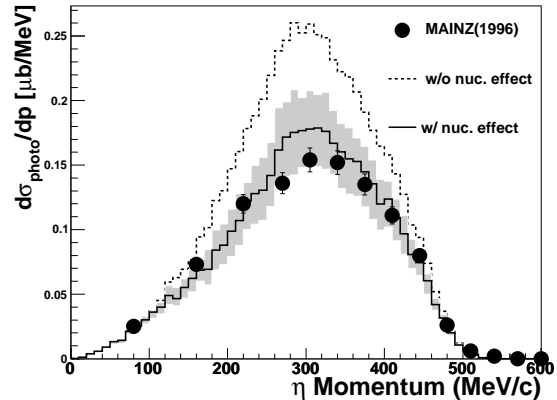


FIG. 2. The differential cross-sections of photoproduction of an η meson on a ^{12}C target with γ energy of 735 ~ 765 MeV. The experimental data at MAINZ [29] are shown as circles. The solid line shows the simulated production cross-section, and its shaded region corresponds to a factor 2 difference in the cross-section of η nuclear effects. The dashed line shows the production cross-section without nuclear effects.

$\omega N \rightarrow \pi\pi N'$ and $\omega N \rightarrow \sigma N$. Approximately 53% of ω mesons generated in $p \rightarrow e^+\omega$ decayed in the nucleus. Therefore, the nuclear effects of secondary pions was also considered.

The CBELSA/TAPS collaboration measured the ω photoproduction cross section on the various nucleus targets of C, Ca, Nb and Pb [33]. They extracted the ωN cross section from the photoproduction cross-sections and compared it with the calculated cross-section by Lykasov *et al.*. The cross-section obtained by the experiment is approximately 3 times larger at most than the calculated cross-section. We took this difference as an uncertainty in the cross-section of ω meson nuclear effects.

B. Atmospheric Neutrino Simulation

Atmospheric neutrino interactions are backgrounds for nucleon decay searches in Super-Kamiokande. Charged current single (multi) pion production can be the dominant background source for the search modes. A charged current quasi-elastic scattering can also contribute the background because a nucleon produced by the neutrino interaction can produce pions by hadronic interactions in water. Atmospheric neutrino events were simulated using the NEUT [34] neutrino interaction MC with an atmospheric neutrino flux calculated by Honda *et al.* [35]. Complete details of the simulation are described in [36]. Atmospheric neutrino simulation MC equivalent to a 500-year observation (11.25 megaton-year exposure) were generated to estimate the nucleon decay search background for each SK-I and SK-II. Pure ν_μ to ν_τ oscillation

with $\Delta m^2 = 2.5 \times 10^{-3} \text{ eV}^2$ and $\sin^2 2\theta = 1.0$ was assumed for the estimation.

IV. DATA SET AND DATA REDUCTION

We used data from a 91.7 kiloton-year exposure of 1489.2 live days during SK-I and a 49.2 kiloton-year exposure of 798.6 live days of during SK-II. The data acquisition trigger threshold for this analysis corresponds to a 5.7 MeV electron in SK-I and 8 MeV in SK-II. The trigger rate was about 11 Hz, resulting in approximately 10^6 events every day. Most of those are events caused by a cosmic ray muon, or a low energy background from the radioactivity of materials around the detector wall, or flashing PMTs. Several stages of data reduction were applied to these events before proceeding to further detailed event reconstruction processes that are described in Section V. The details of the data reduction can be found in [36].

For nucleon decay searches, fully contained (FC) events, which have an activity only in the inner detector, were selected by requiring a vertex to be inside the 22.5 kiloton fiducial volume (2m away from the ID detector wall), visible energy to be greater than 30 MeV and no hit-PMT clusters in the outer detector. The rate of FC events was 8.18 ± 0.07 (stat.) events per day for SK-I and 8.26 ± 0.10 (stat.) events per day for SK-II. In total, we obtained 12232 and 6584 FC events in the SK-I and SK-II data, respectively. The background contamination other than atmospheric neutrinos was estimated to be less than 1%.

The same reduction criteria were also applied to the nucleon decay MC. For nucleon decays via the $N \rightarrow e^+$ meson modes, the reduction survival efficiencies were estimated to be greater than 97%. On the other hand, for the $N \rightarrow \mu^+$ (ρ or ω) modes, the survival efficiencies are relatively lower because the muon can be invisible due to the large meson mass, and because the meson sometimes cannot escape from the nucleus or it can be immediately absorbed by nucleons in water. That results in no detectable event signal in a water Cherenkov detector. The reduction survival efficiencies for all of the search modes are shown in Table I.

Mode	SK-I	SK-II	Mode	SK-I	SK-II
$p \rightarrow e^+\pi^0$	>99%	>99%	$p \rightarrow e^+\omega$	>99%	>99%
$p \rightarrow \mu^+\pi^0$	>99%	>99%	$p \rightarrow \mu^+\omega$	93%	94%
$p \rightarrow e^+\eta$	>99%	>99%	$n \rightarrow e^+\pi^-$	>99%	>99%
$p \rightarrow \mu^+\eta$	>99%	>99%	$n \rightarrow \mu^+\pi^-$	>99%	>99%
$p \rightarrow e^+\rho^0$	98%	98%	$n \rightarrow e^+\rho^-$	97%	97%
$p \rightarrow \mu^+\rho^0$	81%	82%	$n \rightarrow \mu^+\rho^-$	83%	84%

TABLE I. The survival efficiency by the data reduction criteria for the nucleon decay MC events in the fiducial volume for SK-I and SK-II. The fiducial volume cut is not included.

V. EVENT RECONSTRUCTION

A. Event Reconstruction for Nucleon Decay Search

Event reconstruction processes were applied to the fully contained events which passed the data reduction. The same reconstruction algorithms were applied both for the observed data and the MC simulation. Most of the processes are common with atmospheric neutrino analyses in Super-Kamiokande. The details of their algorithms are described in [36].

A vertex position was determined by the time-of-flight subtracted timing distribution. Vertex resolutions for the free proton decay events of $p \rightarrow e^+\pi^0$ are 18.1 (20.1) cm in SK-I (SK-II). A particle identification (PID) algorithm classified found Cherenkov rings into shower-type (e -like) or non shower-type (μ -like). This classification basically exploits the ring pattern difference between a fuzzy ring pattern of electromagnetic showers by an electron or a gamma-ray and a sharper Cherenkov ring edge produced by a muon or a charged pion. The misidentification probabilities for the free proton decay MC samples were estimated to be 3.3% (3.4%) and 4.8% (5.4%) for $p \rightarrow e^+\pi^0$ and $p \rightarrow \mu^+\pi^0$ respectively, in SK-I (SK-II). Additionally, for nucleon decay searches expecting a low momentum muon and/or a charged pion, a reconstructed Cherenkov opening angle was also used to improve the PID efficiency.

The momentum of each ring was estimated by the charge detected inside each Cherenkov ring cone. In multi-ring events such as nucleon decay events, Cherenkov photons radiated from different particles pile up in each PMT. The detected charge at each PMT was separated into the contribution from each particle using an expected charge distribution which takes into account light scattering in water, reflection on PMT surfaces and the vertex shift due to the γ 's conversion length. The momentum resolutions for the proton decay MC were estimated by the monochromatic momentum positron of $p \rightarrow e^+\pi^0$ to be 4.9% in SK-I and 6.0% in SK-II, as shown in Fig. 3. Likewise, the muon momentum resolution was found from ($p \rightarrow \mu^+\pi^0$) to be 2.8% in SK-I and 4.1% in SK-II. The momentum of charged pions is more difficult to reconstruct using only the total detected charge because charged pions suffer from interactions with nucleons in the water. The momentum resolution for charged pions was improved by using the Cherenkov opening angle as well as the total charge. The momentum resolution for charged pions in the $n \rightarrow e^+\pi^-$ MC was estimated to be 9.2% (9.7%) in SK-I (SK-II). Figure 4 shows the charged pion momentum distribution in $n \rightarrow e^+\pi^-$, including the smearing of the true pion momentum due to the Fermi motion of a decaying nucleon.

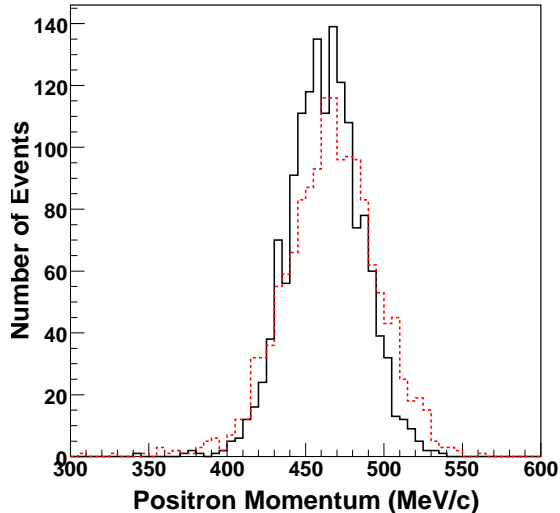


FIG. 3. The reconstructed momentum distributions for positrons in the free proton decay of $p \rightarrow e^+\pi^0$ in SK-I (solid) and SK-II (dashed). The momentum resolution for the positron, as shown by the width of the distribution, is 4.9% in SK-I and 6.0% in SK-II.

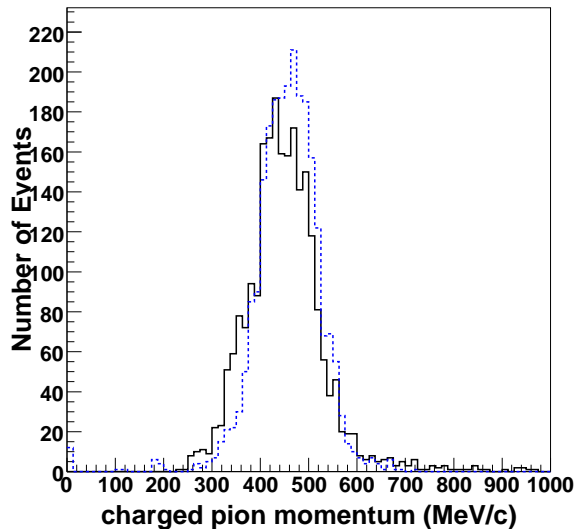


FIG. 4. The charged pion momentum distribution for the $n \rightarrow e^+\pi^-$ MC in SK-I. The solid line and the dashed line show the reconstructed and true pion momentum distributions, respectively. The charged pion momentum can be well reconstructed with a resolution of 9.2% (9.7%) in SK-I (SK-II).

B. Calibration

The characterization of the Super-Kamiokande detector has been performed in a variety of calibrations, which are described in detail in [21, 36]. One of the most important calibrations for nucleon decay searches is the de-

termination of the energy scale because we distinguish nucleon decay events from atmospheric neutrino events using their total invariant mass and momentum.

The absolute momentum scale was checked by the Michel electron momentum spectrum from stopping muons, the invariant mass of π^0 s, and the Cherenkov opening angles and track lengths of stopping muons. The calibrated momentum ranges from a few tens of MeV/c to about 10 GeV/c. The uncertainty of the absolute momentum scale was estimated to be less than 0.74% (1.60%) for SK-I (SK-II). The time variation of the momentum scale was monitored by stopping muon and Michel electron events and estimated to be 0.83% (0.53%) in RMS for SK-I (SK-II).

The detector non-uniformity of the energy scale is also important for the systematic error of the total momentum reconstruction. It was checked by the Michel electron momentum to be uniform within $\pm 0.6\%$ for both SK-I and SK-II.

VI. NUCLEON DECAY ANALYSIS

A. Event Selection

1. Summary of Selection Criteria

The data used in this nucleon decay search are the FC data from the SK-I and SK-II periods. We have to extract only nucleon decay signals from the FC data which are dominated by atmospheric neutrino events. Using the nucleon decay simulation and the atmospheric neutrino simulation, optimal criteria were determined. The atmospheric neutrino MC was normalized with the observed data using the number of single-ring e -like events, which are assumed to have a negligible neutrino oscillation effect. In order to study many nucleon decay modes systematically, event selection criteria were chosen to be as simple and common as possible. The primary for determining the criteria was to obtain a low enough background level.

The following reconstructed information was used in the event selection criteria:

1. the number of Cherenkov rings,
2. the particle type of each ring,
3. the meson invariant mass (if it is possible to be reconstructed),
4. the number of Michel electrons,
5. the total invariant mass and the total momentum (if it is possible to be reconstructed).

The detailed numbers of event selection criteria for all the searches are summarized in Table II.

All of the nucleon decay modes in this study are expected to have multiple Cherenkov rings. The criterion

and efficiency of the number of rings cut for each mode are shown in Table III. More than half of the atmospheric neutrino MC events are single-ring events, as shown in Fig. 5, and they were rejected by the cut on number of rings.

For the particle identification, two types of algorithm were used in this analysis, as described in Section V A. The PID using both a Cherenkov ring pattern and an opening angle was used for the modes in which we search for low momentum muons ($p_\mu < \sim 300$ MeV/ c) or charged pions.

The number of Michel electrons was required to be consistent with a nucleon decay signal. With this requirement, the background events can be effectively reduced, while the loss of the signal detection efficiency is negligible for the modes in which no Michel electrons are expected.

The total momentum P_{tot} , the total energy E_{tot} , and the total invariant mass M_{tot} are defined as:

$$P_{\text{tot}} = \left| \sum_i^{\text{all}} \vec{p}_i \right|, \quad (3)$$

$$E_{\text{tot}} = \sum_i^{\text{all}} \sqrt{|\vec{p}_i|^2 + m_i^2}, \quad (4)$$

$$M_{\text{tot}} = \sqrt{E_{\text{tot}}^2 - P_{\text{tot}}^2}, \quad (5)$$

where \vec{p}_i is the momentum of each Cherenkov ring, and m_i is the mass of a particle (γ , e^\pm , μ^\pm , π^\pm). The meson mass is reconstructed in a similar way by summing up the momenta and energies of secondary particles from the meson decay. Although our particle identification algorithm can only classify a Cherenkov ring into a shower-type ring (e^\pm or γ) or a non shower-type ring (μ^\pm or π^\pm), the invariant mass reconstruction in some modes requires the ability to distinguish e^\pm from γ or μ^\pm from π^\pm . For example, for the π^0 invariant mass reconstruction in the $p \rightarrow e^+\pi^0$ mode search, we should identify each Cherenkov ring as originating from a positron or a γ -ray. However, that cannot be done in a large water Cherenkov detector. In these cases, the invariant mass was calculated for all possible combinations of particle type assignment. Then, the best combination in which the reconstructed mass is the closest to the expected nucleon (or meson) mass, is selected. All of the studied nucleon decay modes are two-body decays with back-to-back kinematics, and have isotropic event signatures, which is the most significant difference from typical atmospheric neutrino events. Therefore, the event selection by total momentum and total invariant mass is a powerful tool to eliminate the atmospheric neutrino background as can be found in Fig. 6. The total momentum cut threshold is set to be 250 MeV/ c for most searches considering the Fermi motion of bound nucleons. To keep the background rates low enough (below 0.5 events in the total exposure), a tighter total momentum cut with a threshold of 150 (or 200) MeV/ c is applied in some relatively high-background mode searches.

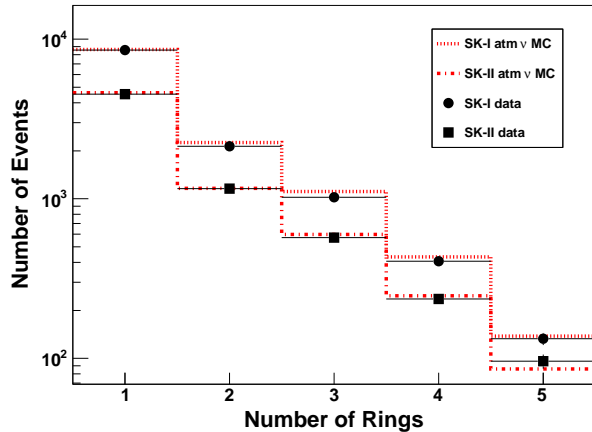


FIG. 5. Number of rings distribution for atmospheric neutrino MC and data. The number of MC events are normalized to the observed data by the number of single ring e -like events (also in other figures unless otherwise noted).

2. $p \rightarrow l^+\pi^0$ Mode Search

In the proton decay of $p \rightarrow e^+\pi^0$ ($p \rightarrow \mu^+\pi^0$), a neutral pion and a positron (muon) are back-to-back and have the same momentum of 459 (453) MeV/ c in the proton rest frame. The neutral pion immediately decays into two γ -rays. Figure 7 shows the event signature of a typical proton decay MC event for $p \rightarrow e^+\pi^0$. One shower-type ring from the positron and two shower-type rings from the π^0 are clearly seen in this figure.

The two γ -rays from the π^0 decay are back-to-back in the π^0 rest frame. They are Lorentz-boosted by the π^0 momentum of ~ 450 MeV/ c , so the momentum of one of the two γ -rays in the laboratory frame can be very low depending on the direction of the Lorentz boost. In such a case, it sometimes happens that only one ring from π^0 decay is identified. For free proton decays of $p \rightarrow e^+\pi^0$, the fraction of two-ring and three-ring events identified was 39% and 60%, respectively.

If all three rings were found, the π^0 invariant mass, which is reconstructed by two of the three rings, was required to be between 85 and 185 MeV/ c . The reconstructed π^0 invariant mass distribution for the proton decay MC is shown in Fig. 8. For free proton decay events of $p \rightarrow e^+\pi^0$, the mean of the reconstructed π^0 invariant mass is 137 MeV/ c^2 , and its resolution is 20 MeV/ c^2 .

The final criterion of total invariant mass and momentum selects the events which are consistent with the momentum and mass of a parent proton. Figure 9 shows the distribution of the total invariant mass. For free proton decay events, the total invariant mass was well reconstructed. The resolution of the total invariant mass distribution is 28.2 (36.2) MeV/ c^2 in SK-I (SK-II). The resolution of the total momentum is 29.8 (32.5) MeV/ c . The total momentum and invariant mass cut was wide

Modes	(1) Ring	(2) PID	(3) M_{meson}	(4) decay- e	(5) M_{tot}	P_{tot}	Note
$p \rightarrow e^+ \pi^0$	2, 3	SS(S)	85~185 (π^0)	0	800~1050	<250	
$p \rightarrow \mu^+ \pi^0$	2, 3	NS(S)	85~185 (π^0)	1	800~1050	<250	
$p \rightarrow e^+ \eta$ (2γ)	3	SSS	480~620 (η)	0	800~1050	<250	
$p \rightarrow \mu^+ \eta$ (2γ)	3	NSS*	480~620 (η)	1	800~1050	<250	
$p \rightarrow e^+ \eta$ ($3\pi^0$)	4, 5	SSSS(S)	400~700 (η)	0	800~1050	<150	
$p \rightarrow \mu^+ \eta$ ($3\pi^0$)	4, 5	NSSS(S)*	400~700 (η)	1	800~1050	<250	
$p \rightarrow e^+ \rho^0$	3	SNN*	600~900 (ρ^0)	0, 1	800~1050	<150	
$p \rightarrow \mu^+ \rho^0$	3	NNN*	600~900 (ρ^0)	1, 2	800~1050	<250	
$p \rightarrow e^+ \omega$ ($\pi^0 \gamma$)	3, 4	SSS(S)	650~900 (ω)	0	800~1050	<150	
$p \rightarrow \mu^+ \omega$ ($\pi^0 \gamma$)	2, 3	SS(S)	650~900 (ω)	1	-	<200	
$p \rightarrow e^+ \omega$ ($\pi^+ \pi^- \pi^0$)	4	SSSN*	85~185 (π^0)	0, 1	600~800	<200	P_{e^+}
$p \rightarrow \mu^+ \omega$ ($\pi^+ \pi^- \pi^0$)	3	SSN*	85~185 (π^0)	2	450~700	<200	
$n \rightarrow e^+ \pi^-$	2	SN	-	0	800~1050	<250	
$n \rightarrow \mu^+ \pi^-$	2	NN	-	1	800~1050	<250	
$n \rightarrow e^+ \rho^-$	4	SSSN*	600~900 (ρ^-)	0	800~1050	<250	M_{π^0}
$n \rightarrow \mu^+ \rho^-$	3	SSN*	600~900 (ρ^-)	1	-	<150	M_{π^0}

TABLE II. Summary of the selection criteria. The numbers in parentheses correspond to the numbers of selection criteria described in Section VIA 1. For example, for the $p \rightarrow \mu^+ \eta$ ($3\pi^0$) mode, this table means that the selection criteria requires that (1) the number of Cherenkov rings is 4 or 5, (2) one ring is non shower-type and all other rings are shower-type, (3) reconstructed η meson invariant mass is in between 400 and 700 MeV/c^2 , (4) the number of Michel electron is 1, and (5) reconstructed total invariant mass is in between 800 and 1050 MeV/c^2 and reconstructed total momentum is less than 250 MeV/c . S and N in the PID column stand for shower-type rings and non shower-type rings, respectively. Asterisks in PID indicate that a PID using both Cherenkov ring pattern and opening angle was used for identifying low momentum muons ($p_\mu < \sim 300 \text{ MeV}/c$) or charged pions. All the invariant mass and momenta are written in units of MeV/c^2 and MeV/c , respectively. For the $p \rightarrow e^+ \omega$ (3π) mode, a positron momentum cut is applied ($100 < P_{e^+} < 200$). For the $n \rightarrow l^+ \rho^-$ mode, a π^0 invariant mass cut is also applied.

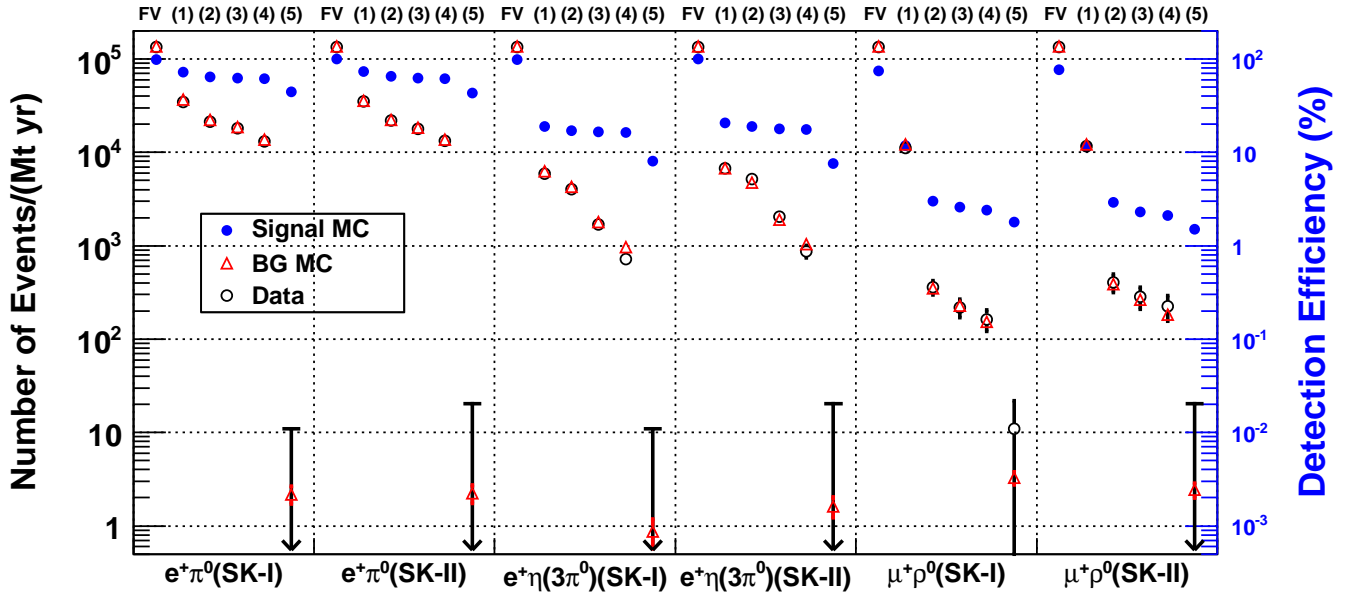


FIG. 6. Number of events and detection efficiency at each event selection step: (FV) fiducial volume, (1) number of Cherenkov rings, (2) PID, (3) meson invariant mass, (4) number of Michel electrons and (5) total invariant mass and total momentum. The plot shows three nucleon decay mode searches: the mode with highest efficiency ($p \rightarrow e^+ \pi^0$), the mode with the greatest number of rings ($p \rightarrow e^+ \eta$ ($\eta \rightarrow 3\pi^0$)) and the mode using PID with both Cherenkov ring pattern and opening angle ($p \rightarrow \mu^+ \rho^0$). The number of observed events and the estimated background rates agree with each other. Also, the searches in SK-I and SK-II are compared.

Mode	N_{ring}	Efficiency %	
		SK-I	SK-II
$p \rightarrow e^+\pi^0$	2 or 3	73 (98)	74 (98)
$p \rightarrow \mu^+\pi^0$	2 or 3	74 (98)	74 (98)
$p \rightarrow e^+\eta (2\gamma)$	3	44 (92)	45 (89)
$p \rightarrow \mu^+\eta (2\gamma)$	3	44 (91)	44 (89)
$p \rightarrow e^+\eta (3\pi^0)$	4 or 5	19 (76)	21 (76)
$p \rightarrow \mu^+\eta (3\pi^0)$	4 or 5	22 (82)	21 (81)
$p \rightarrow e^+\rho^0$	3	26 (50)	26 (47)
$p \rightarrow \mu^+\rho^0$	3	12 (26)	11 (25)
$p \rightarrow e^+\omega (\pi^0\gamma)$	3 or 4	58 (93)	59 (89)
$p \rightarrow \mu^+\omega (\pi^0\gamma)$	2 or 3	61 (97)	61 (96)
$p \rightarrow e^+\omega (3\pi)$	4	19 (27)	19 (26)
$p \rightarrow \mu^+\omega (3\pi)$	3	27 (41)	26 (39)
$n \rightarrow e^+\pi^-$	2	49	49
$n \rightarrow \mu^+\pi^-$	2	49	49
$n \rightarrow e^+\rho^-$	4	9	9
$n \rightarrow \mu^+\rho^-$	3	17	17

TABLE III. Efficiency of cut on number of rings for nucleon decay MC for SK-I and SK-II. Numbers in parentheses are efficiencies for free proton decay events. These efficiencies include the efficiency for the FC data reduction and the fiducial volume cut.

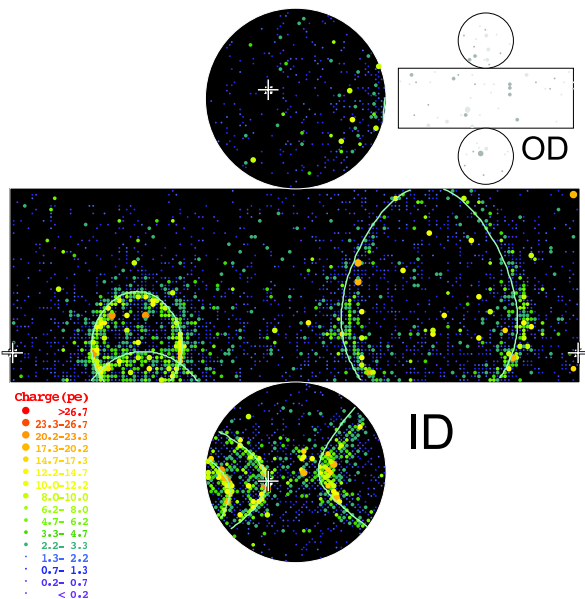


FIG. 7. A typical proton decay MC event of $p \rightarrow e^+\pi^0$ in SK-I. One Cherenkov ring from a positron and two Cherenkov rings from the two γ -rays from π^0 decay can be observed on the right and the left of the figure, respectively. The size of circles indicate the amount of detected charge. The crosses on the plot show a reconstructed vertex position horizontally and vertically projected on the detector wall. Solid lines show the reconstructed rings. The reconstruction algorithms correctly find all rings and identify their particle for this event.

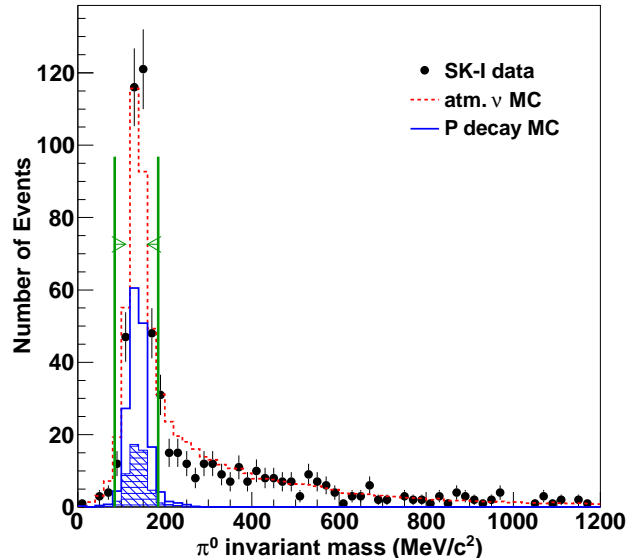


FIG. 8. The invariant mass of π^0 distributions for SK-I proton decay MC ($p \rightarrow e^+\pi^0$), atmospheric neutrino MC, and SK-I data. The shaded histogram is the distribution of free proton decay events. The bars and arrows indicate the π^0 invariant mass cut threshold.

enough for free proton decay events. The total momentum and total invariant mass distributions of the proton decay MC and the atmospheric neutrino MC are clearly different from each other, as shown in Fig. 10. This criterion reduces the atmospheric neutrino background by more than three orders of magnitude, as shown in Fig. 6.

The detection efficiency for $p \rightarrow e^+\pi^0$ was estimated to be 44.6 (43.5)% in SK-I (SK-II). The inefficiency is mainly due to nuclear interaction effects of pions in ^{16}O . For free proton decay events, high efficiencies of 87% (86%) were achieved for $p \rightarrow e^+\pi^0$. As for the $p \rightarrow \mu^+\pi^0$ mode search, differences in the selection criteria from the $p \rightarrow e^+\pi^0$ mode are the requirement of one non shower-type ring and one Michel electron. The detection efficiency for a Michel electron from the decay of μ was approximately 80%. This is the reason for the detection efficiency difference between $p \rightarrow e^+\pi^0$ and $p \rightarrow \mu^+\pi^0$. The detection efficiency for the $p \rightarrow \mu^+\pi^0$ mode was estimated to be 35.5% (34.7%) in SK-I (SK-II).

The background events for $p \rightarrow e^+\pi^0$ and $p \rightarrow \mu^+\pi^0$ were estimated to be 0.31 and 0.34 events in total for SK-I and SK-II, respectively. The background rates for $p \rightarrow e^+\pi^0$ in SK-I and SK-II are 2.1 and 2.2 events/(megaton-years), respectively. Therefore, low-background observations with high efficiency were achieved for these modes in the Super-Kamiokande detector, both in the SK-I and SK-II periods. The background for $p \rightarrow e^+\pi^0$ was also estimated from the experimental data of the K2K ν beam and 1-kiloton wa-

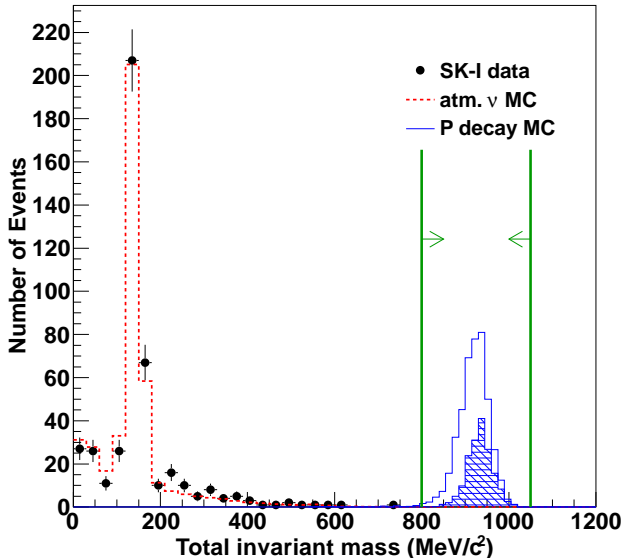


FIG. 9. The total invariant mass distributions for proton decay MC ($p \rightarrow e^+\pi^0$), atmospheric neutrino MC, and observed data in SK-I. The shaded histogram is the distribution of free proton decay events. The bars and arrows indicate the total invariant mass cut threshold. Only events which satisfy all other selection criteria except this are plotted. The distribution of atmospheric neutrino MC has the π^0 invariant mass peak, which is consistent with the observed data.

ter Cherenkov detector [37]. The number of expected background events estimated from the K2K data is $0.23_{-0.05}^{+0.06}(\text{stat.})_{-0.07}^{+0.06}(\text{sys.})$ events for the exposure of SK-I plus SK-II, which is consistent with the estimate from our MC. The background estimate was also compared with a different neutrino interaction MC, NUANCE [38]. The number of background events estimated by NUANCE was 0.27 ± 0.10 events (in SK-I+SK-II), which is also consistent with our primary estimate. These results are summarized in Table IV with the results of all the other studied modes.

3. $p \rightarrow l^+\eta$ Mode Search

The η meson has three dominant decay modes; we search for two of the three modes: $\eta \rightarrow 2\gamma$ ($Br=39\%$) and $\eta \rightarrow 3\pi^0$ ($Br=33\%$).

The mass of η meson is $548 \text{ MeV}/c^2$. Because its mass is larger than the π^0 mass, the generated charged lepton and η meson have smaller momentum, $\sim 300 \text{ MeV}/c$ in the proton rest frame, compared with the momentum of generated particles in the $p \rightarrow l^+\pi^0$ modes. For the $p \rightarrow \mu^+\eta$ mode, PID with Cherenkov ring pattern and opening angle was used to improve the PID for a low momentum μ ring. This is common for both meson decay

modes of $p \rightarrow \mu^+\eta$.

Figure 11 shows the total momentum and total invariant mass distributions of the $p \rightarrow l^+\eta$ modes. Compared with the $p \rightarrow l^+\pi^0$ modes many fewer events in both the atmospheric neutrino MC and observed data survive the selection criteria except for the total momentum and invariant mass cut. That is because a significant number of atmospheric neutrino events with π^0 production can survive the selection criteria (except for the total momentum and invariant mass cut) for the $p \rightarrow l^+\pi^0$ modes while the number of atmospheric neutrino events with η production are negligible.

a. $p \rightarrow l^+\eta$ ($\eta \rightarrow 2\gamma$) Mode These modes have very similar event signatures with $p \rightarrow e^+\pi^0$ and $p \rightarrow \mu^+\pi^0$. However, the momentum of the two γ -rays in the η meson rest frame is $274 \text{ MeV}/c$, which is much larger than that in $p \rightarrow e^+\pi^0$ and $p \rightarrow \mu^+\pi^0$. The opening angle between the two γ -rays from the η meson decay is about 132 degrees in the laboratory frame. Therefore, three Cherenkov rings are clearly visible and can easily be separated so that the number of Cherenkov rings is required to be three. The fraction of three-ring events in the free proton decay event is greater than 90%.

Because only the three-ring events survive the number of rings cut, an η invariant mass cut was applied to all of the surviving events. Figure 12 (left panels) shows the reconstructed invariant mass of the η meson for the proton decay MC in the $p \rightarrow e^+\eta$ mode. The η invariant mass was well reconstructed.

b. $p \rightarrow l^+\eta$ ($\eta \rightarrow 3\pi^0$) Mode In these proton decay modes, the η meson decays into three π^0 s, and the three π^0 s immediately decay into six γ -rays. Therefore, one ring from a charged lepton and six rings from the γ -rays can be observed in principle. However, our Cherenkov ring counting algorithm is only capable of finding up to five rings. Consequently, the criterion of the number of rings was applied to select events with four or five rings. In SK-I free proton decay events of the $\eta \rightarrow 3\pi^0$ mode of $p \rightarrow e^+\eta$ ($p \rightarrow \mu^+\eta$), 77% (84%) of the events satisfy the criterion.

The invariant mass of the η meson was reconstructed using only three or four shower-type rings, though there should be 6 rings from the $3\pi^0$ s. This resulted in a worse invariant mass resolution for the η meson. Therefore, the event selection window of the η invariant mass was larger than that in the search via the $\eta \rightarrow 2\gamma$ mode as shown in Table II.

As shown in Fig. 11, the background rates for $p \rightarrow e^+\eta$ (3π) were not low enough if the standard event selection criteria of $P_{\text{tot}} < 250 \text{ MeV}/c$ was applied. In order to further reduce the background, the tighter total momentum cut of $P_{\text{tot}} < 150 \text{ MeV}/c$ was applied for the $p \rightarrow e^+\eta$ mode.

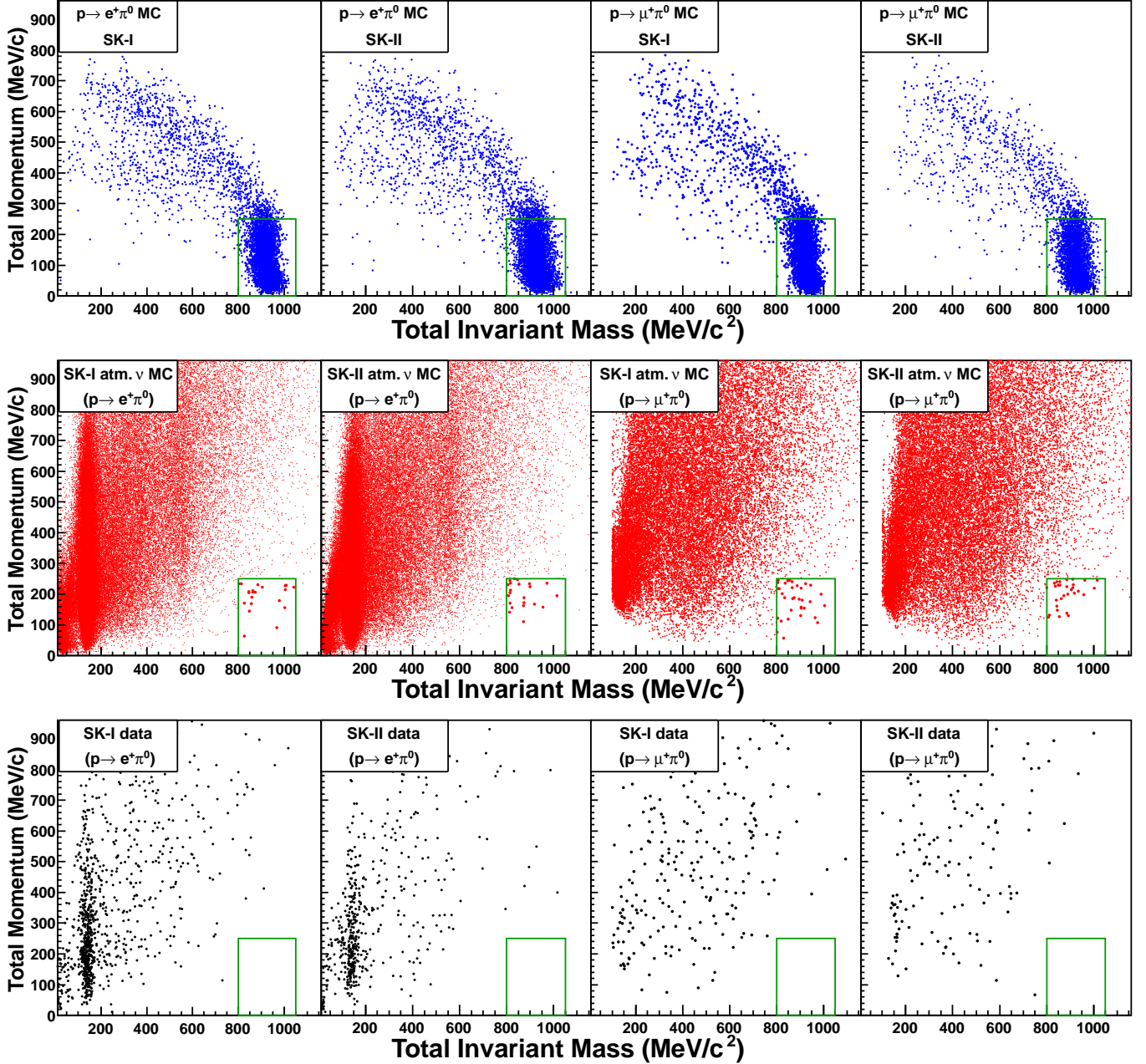


FIG. 10. Total momentum versus total invariant mass distributions, from left to right: SK-I $p \rightarrow e^+\pi^0$; SK-II $p \rightarrow e^+\pi^0$; SK-I $p \rightarrow \mu^+\pi^0$; and SK-II $p \rightarrow \mu^+\pi^0$, from top to bottom: the proton decay MC; the atmospheric neutrino MC (11.25 megaton-years for each SK-I and SK-II); and the observed data (91.7 kiloton-years in SK-I and 49.2 kiloton-years in SK-II). These events satisfy the event selection criteria except for the selection by the total momentum and total mass. The boxes in figures indicate the total momentum and mass criteria. The points in the boxes of the atmospheric neutrino MC are shown in a larger size to show the distributions in the signal box. No candidates were found for either $p \rightarrow e^+\pi^0$ or $p \rightarrow \mu^+\pi^0$ in the data.

4. $p \rightarrow l^+\omega$ Mode Search

Two of the ω meson decay modes were searched for in this study. One is the $\omega \rightarrow \pi^+\pi^-\pi^0$ mode ($Br=89\%$), and the other is the $\omega \rightarrow \pi^0\gamma$ mode ($Br=9\%$). The momentum of a generated charged lepton and an ω meson

is 143 (105) MeV/ c^2 in $p \rightarrow e^+\omega$ ($p \rightarrow \mu^+\omega$). For the $p \rightarrow \mu^+\omega$ mode, the muon momentum is lower than the Cherenkov threshold, and the muon ring cannot be observed. Therefore, the existence of the muon is indicated only by detection of the Michel electron from the muon decay. The ω meson suffers from nuclear effects in the

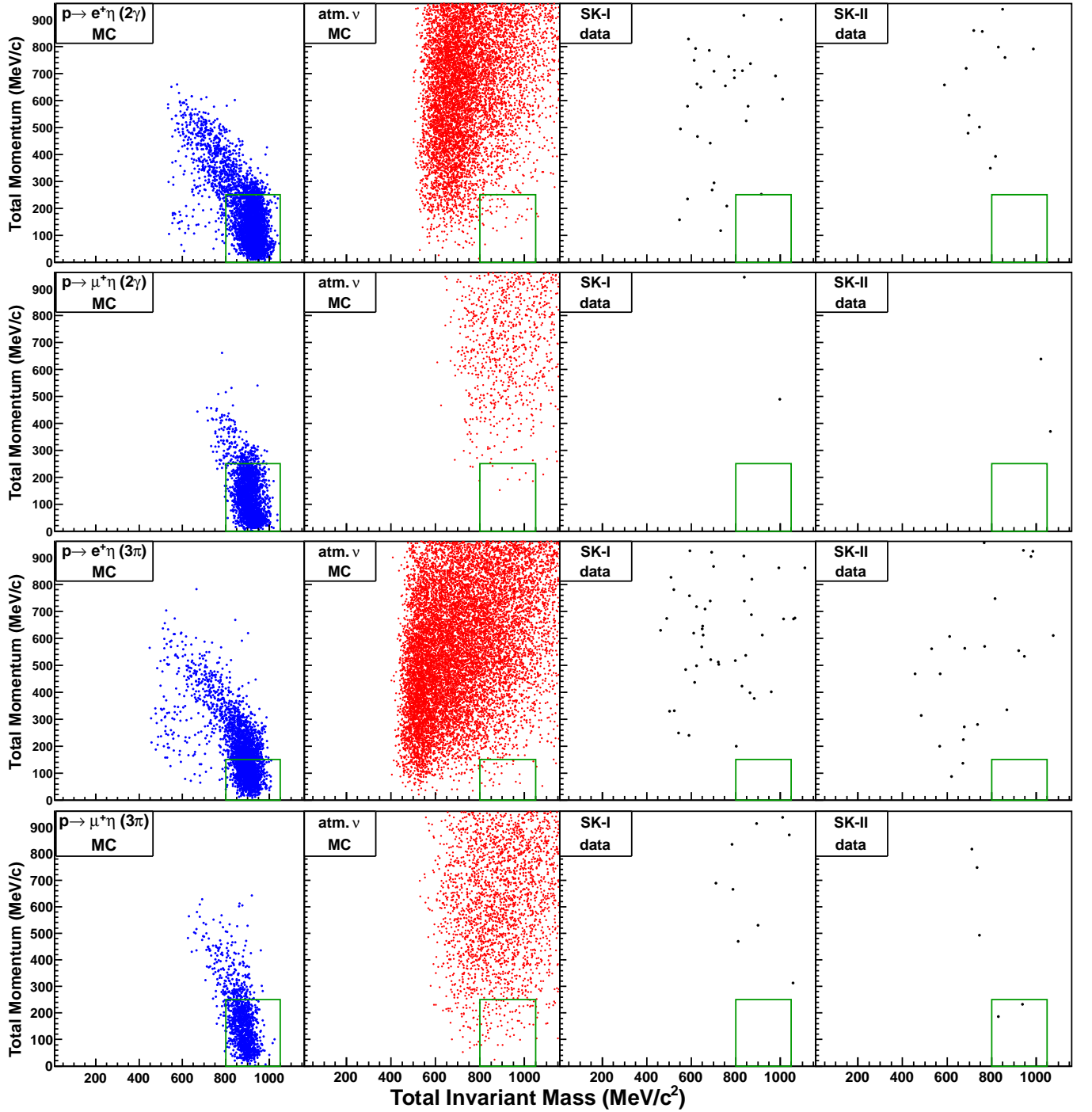


FIG. 11. Total momentum versus total invariant mass distributions of proton decay MC (SK-I+II combined), the atmospheric neutrino MC (SK-I+II combined; 11.25 megaton-years for each SK-I and SK-II) and SK-I (91.7 kiloton-years) and SK-II (49.2 kiloton-years) data, from top to bottom: $p \rightarrow e^+\eta (2\gamma)$, $p \rightarrow \mu^+\eta (2\gamma)$, $p \rightarrow e^+\eta (3\pi^0)$ and $p \rightarrow \mu^+\eta (3\pi^0)$. The boxes in figures indicate the total momentum and mass criteria. These events satisfy the event selection criteria for each mode except for the selection on the total momentum and total mass. Two candidates for $p \rightarrow \mu^+\eta (3\pi^0)$ were found in the SK-II data.

case of a decay in an ^{16}O nucleus. Only $\sim 20\%$ of the ω mesons could escape from the nucleus. This causes the inefficiency for these two search modes.

a. $p \rightarrow l^+\omega (\omega \rightarrow \pi^0\gamma)$ Mode In the $\omega \rightarrow \pi^0\gamma$ decay mode, the π^0 decays into two γ -rays, and three shower-type rings can be observed from the decays of the ω meson. The π^0 momentum from the ω decay is approxi-

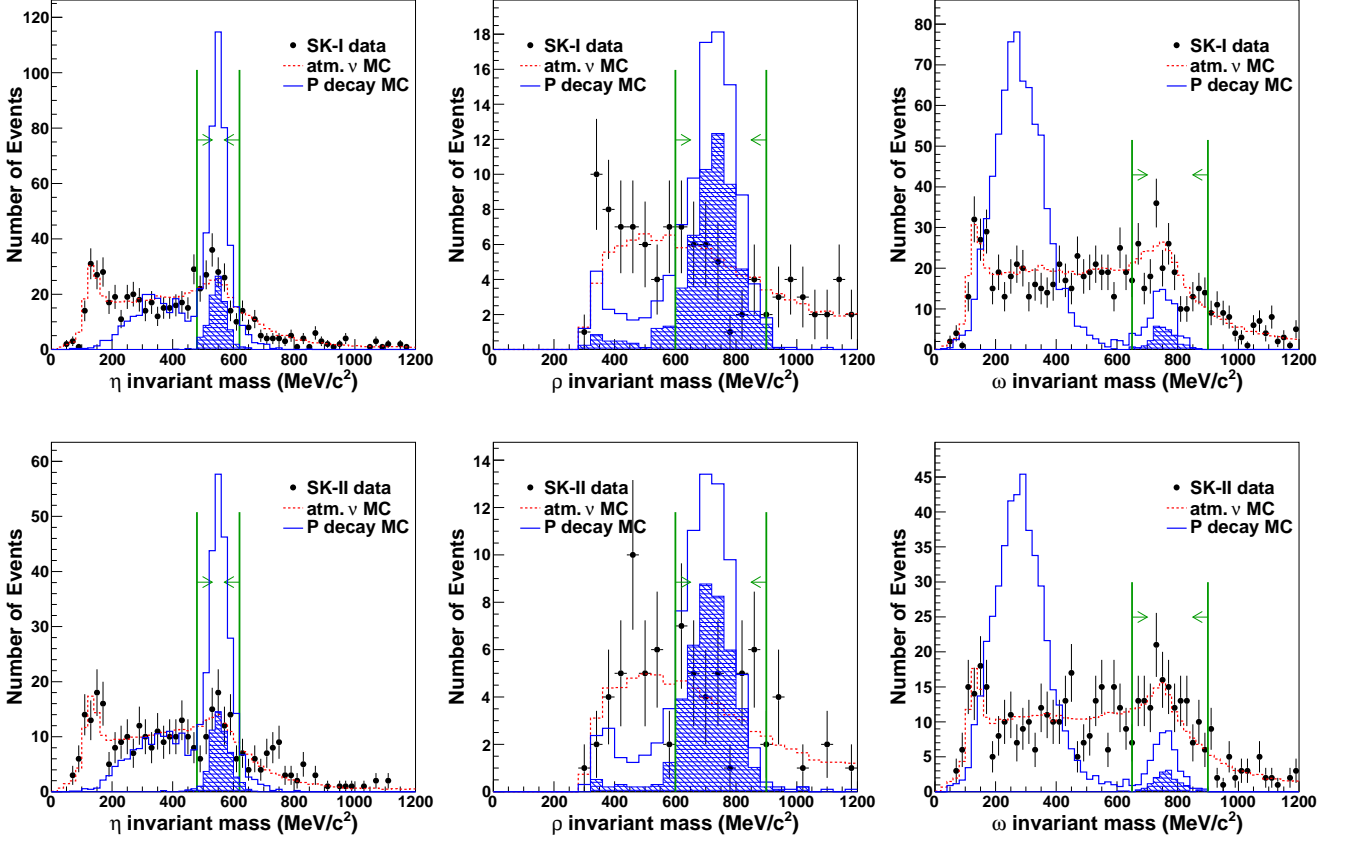


FIG. 12. The meson invariant mass distributions for the proton decay MC (solid lines), the atmospheric neutrino MC (dashed lines) and the observed data (points) in SK-I (top) and SK-II (bottom), from left to right; $p \rightarrow e^+\eta$ mode (2γ), $p \rightarrow e^+\rho^0$ mode and $p \rightarrow e^+\omega$ mode ($\pi^0\gamma$). Free proton decay events are indicated by shaded histograms. All decay branches of the mesons are filled in the histograms for the proton decay MCs. The other peaks outside of the selection window are events from the other decay branches.

mately $380 \text{ MeV}/c$ in the ω meson rest frame. For same reason as in $p \rightarrow e^+\pi^0$ or $p \rightarrow \mu^+\pi^0$, one of the two rings from the π^0 decay has a certain probability of not being identified. Therefore, two or three shower-type rings were required from the ω meson decay, and one more shower-type rings from e^+ was required only in the case of the $p \rightarrow e^+\omega$ mode. The fraction of events with 3 or 4 rings (2 or 3 rings) was 95% (97%) for the SK-I free proton decay of the $\omega \rightarrow \pi^0\gamma$ mode for $p \rightarrow e^+\omega$ ($p \rightarrow \mu^+\omega$).

The ω invariant mass was reconstructed using all detected rings for the $p \rightarrow \mu^+\omega$ mode. For the $p \rightarrow e^+\omega$ mode, the invariant mass was reconstructed by all but one of the detected rings, which was assumed to be e^+ ring. The ω invariant mass distribution for the proton decay MC is shown in the right panels of Fig. 12. The lower invariant mass peak in the proton decay MC was due to the another ω meson decay mode of $\omega \rightarrow \pi^+\pi^-\pi^0$.

Since the muon is invisible for the $p \rightarrow \mu^+\omega$ mode, the total momentum corresponds not to the proton momentum, but to the ω meson momentum. Thus, the reconstructed momentum for the free proton decay in

SK-I peaked around $100 \text{ MeV}/c$, which can be seen in Fig. 13. In order to eliminate the background sufficiently, tighter total momentum cuts were applied for both modes: $P_{\text{tot}} < 150 \text{ MeV}/c$ for $p \rightarrow e^+\omega$ and $P_{\text{tot}} < 200 \text{ MeV}/c$ for $p \rightarrow \mu^+\omega$. The sharp cutoffs in the total invariant mass distributions for $p \rightarrow \mu^+\omega$ ($\pi^0\gamma$) in Fig. 13 correspond to the ω invariant mass cut. There is no total invariant mass cut applied to this mode.

b. $p \rightarrow l^+\omega$ ($\omega \rightarrow \pi^+\pi^-\pi^0$) Mode In this ω decay mode, the ω decays into two low momentum charged pions and a neutral pion. Their momenta are about $220 \text{ MeV}/c$. In order to find the low momentum non shower-type ring, PID with both a Cherenkov ring pattern and an opening angle was used for these modes. Due to the strong interaction of charged pions in water, finding both of the charged pion rings is difficult. Therefore, we required finding only one of the two charged pion rings. For the $p \rightarrow e^+\omega$ ($p \rightarrow \mu^+\omega$) mode, 4 (3) rings were required to be found in total. The efficiency of the number of rings cut was 27% (42%) for SK-I free proton decay MC of the $p \rightarrow e^+\omega$ ($p \rightarrow \mu^+\omega$), $\omega \rightarrow \pi^+\pi^-\pi^0$

mode.

Since one of the two charged pions was assumed to be invisible in the selection criteria, the invariant mass of the ω and the proton cannot be reconstructed. Instead of the ω mass reconstruction, the reconstructed π^0 invariant mass was required to be consistent with π^0 mass. As for the total invariant mass, the event selection criteria for the total mass were set to be lower than the normal event selection criteria, as shown in Fig. 13 and Table II. The selection windows were determined to reduce the atmospheric neutrino MC, though they were not wide enough to also allow in the free proton decay events.

For the $p \rightarrow \mu^+\omega$ mode, both Michel electrons from the decay of μ^+ and π^+ were required to be found. Although the detection efficiency is decreased by a factor of 2, this cut reduced the background by an order of magnitude.

In order to reduce the background further, the reconstructed positron momentum was also required to be consistent with the positron momentum for the $p \rightarrow e^+\omega$ mode. This criterion reduced the background by a factor of 2, while the detection efficiency was decreased by about 20%.

5. $p \rightarrow l^+\rho^0$ Mode Search

In the proton decay of $p \rightarrow e^+\rho^0$ and $p \rightarrow \mu^+\rho^0$, the momentum of the charged lepton and ρ meson, which depends on the ρ meson mass with a width of $\Gamma = 149$ MeV, is about 170 MeV/ c . For $p \rightarrow \mu^+\rho^0$, the muon momentum can be lower than the Cherenkov threshold. The ρ meson decays into $\pi^+\pi^-$ with a branching ratio of $\sim 100\%$. The two pions suffer from strong interactions with nucleons in water, and also in the nucleus in the case of a proton decay in an ^{16}O nucleus. Accordingly, a probability for finding all three Cherenkov rings from the charged lepton and the two charged pions is intrinsically very low. However, in order to reduce the background in the selection by total invariant mass and total momentum, all three rings were required to be found in order to reconstruct the mass and the momentum of the proton. The fraction of three-ring events was 50% and 27% for the free proton decay of $p \rightarrow e^+\rho^0$ and $p \rightarrow \mu^+\rho^0$, respectively. The lower efficiency for $p \rightarrow \mu^+\rho^0$ was due to proton decay events with an invisible muon.

The charged pions from the decay of the ρ meson have a low momentum of about 300 MeV/ c . Therefore, PID with both Cherenkov ring pattern and opening angle was used for both $p \rightarrow e^+\rho^0$ and $p \rightarrow \mu^+\rho^0$.

The invariant mass of the ρ meson was reconstructed by two non shower-type rings and required to be between 600 and 900 MeV/ c^2 , as shown in the center panels of Fig. 12. Most of the events shown in ρ meson distributions were from free proton decay events. This means that the events from proton decays in an ^{16}O nucleus rarely survived the selection criteria on the number of rings and the PID.

For these mode searches, one extra Michel electron is

expected from the π^+ decay, in addition to the one Michel electron from the μ decay. The number of Michel electrons were required to be consistent with this expectation.

The total momentum and total invariant mass distributions for the $p \rightarrow l^+\rho^0$ modes are shown in Fig. 14. The $p \rightarrow e^+\rho^0$ mode had a relatively higher background rate than that of $p \rightarrow \mu^+\rho^0$ mode. In order to reduce the background, a tighter total momentum cut of $P_{\text{tot}} < 150$ MeV/ c was applied for the $p \rightarrow e^+\rho^0$ mode.

6. $n \rightarrow l^+\rho^-$ Mode Search

All of the neutrons in an H_2O molecule are bound in a nucleus. Because of this, all generated charged pions in neutron decay modes suffer from nuclear effects, and detection efficiencies for neutron decay searches tend to be lower compared with their corresponding proton decay searches.

In the neutron decay of $n \rightarrow l^+\rho^-$, the ρ^- meson decays into $\pi^-\pi^0$. The π^0 decays into two γ -rays. Accordingly, two shower-type rings and one non shower-type ring were required from the ρ^- meson decay. One more shower-type ring from the positron was required for the $n \rightarrow e^+\rho^-$ mode search, while one more non shower-type ring from the muon was not required for the $n \rightarrow \mu^+\rho^-$ mode search. In order to find the low momentum non shower-type ring, the PID with both a Cherenkov ring pattern and an opening angle was used for these modes. The fraction of 4-ring (3-ring) events was 9% (23%) for $n \rightarrow e^+\rho^-$ ($n \rightarrow \mu^+\rho^-$).

The invariant mass of the ρ^- meson was reconstructed using two shower-type rings and one non shower-type ring and required to be between 600 and 900 MeV/ c^2 . In addition to the ρ meson mass, a π^0 invariant mass cut was also applied. This additional cut reduced the atmospheric neutrino background by a factor of 2, while the loss of detection efficiency was about 10%.

The total momentum and total invariant mass distributions for the $n \rightarrow l^+\rho^-$ modes are shown in Fig. 14. The tighter total momentum cut of $P_{\text{tot}} < 150$ MeV/ c was applied to reduce the background for the $n \rightarrow \mu^+\rho^-$ mode because the nucleon invariant mass cannot be reconstructed for this mode due to the invisible muon.

7. $n \rightarrow l^+\pi^-$ Mode Search

The momentum of the charged lepton and charged pion in this mode is about 460 MeV/ c , almost the same as that of $p \rightarrow l^+\pi^0$. In these modes, a Cherenkov ring from the charged pion generated from the nucleon decay can be observed. Approximately 50% of the neutron decay events in SK-I were 2-ring events from the charged lepton and the charged pion. There was no event selection on the meson invariant mass for these modes.

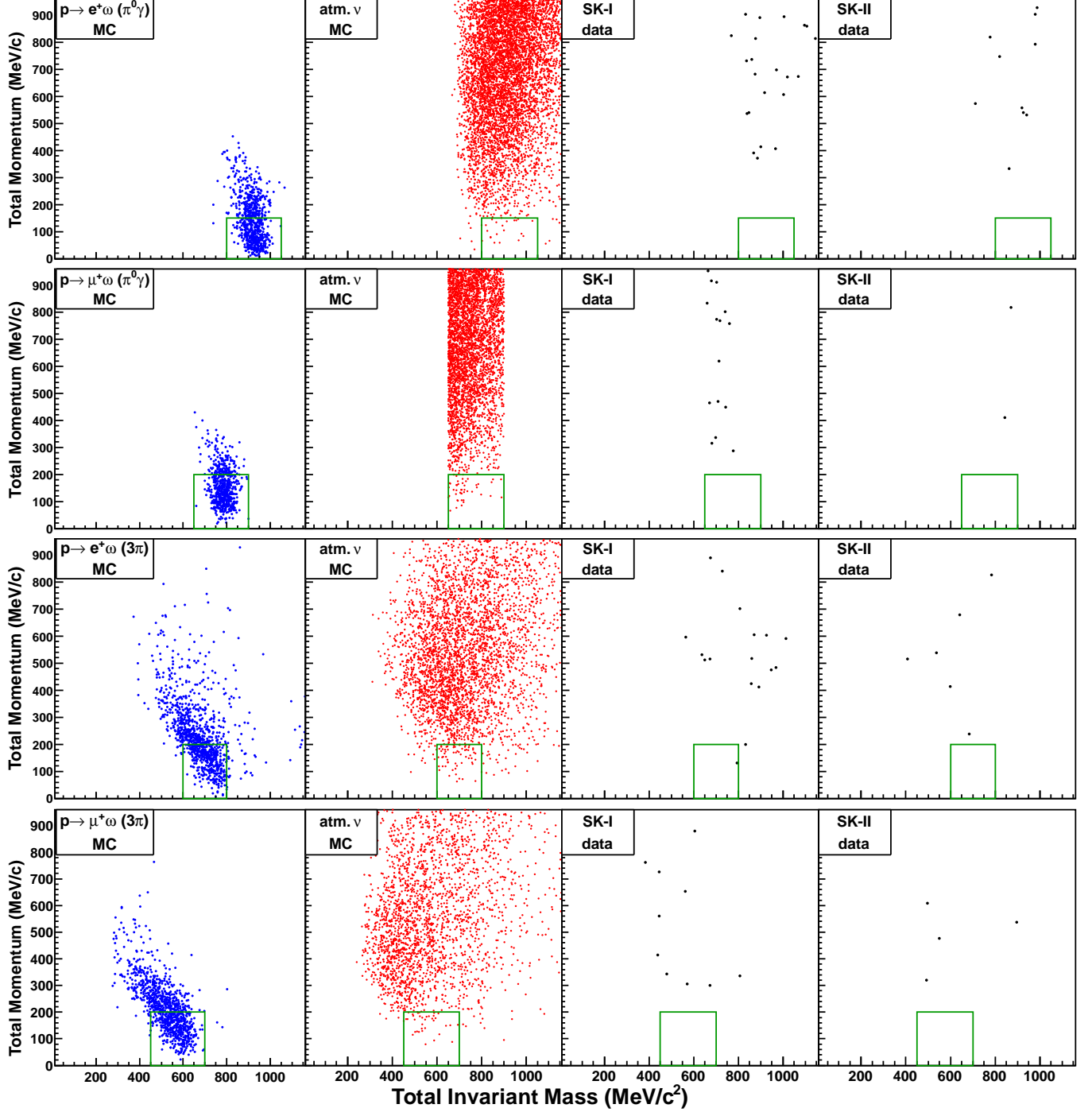


FIG. 13. Total momentum versus total invariant mass distributions of proton decay MC (SK-I+II combined), the atmospheric neutrino MC (SK-I+II combined; 11.25 megaton-years for each SK-I and SK-II) and SK-I (91.7 kiloton-years) and SK-II (49.2 kiloton-years) data, from top to bottom: $p \rightarrow e^+\omega (\pi^0\gamma)$, $p \rightarrow \mu^+\omega (\pi^0\gamma)$, $p \rightarrow e^+\omega (3\pi)$ and $p \rightarrow \mu^+\omega (3\pi)$. These events satisfy the event selection criteria for each mode except for the selections on the total momentum and total mass. The boxes in the figures indicate the total momentum and mass criteria. For the $p \rightarrow \mu^+\omega (\pi^0\gamma)$ mode, the total invariant mass is equivalent to the meson invariant mass because a muon is invisible. The sharp cutoffs in the total invariant mass distribution correspond to the ω invariant mass cut. For the $p \rightarrow \mu^+\omega (3\pi)$ mode, there are no such sharp cutoffs because the ω invariant mass cut is not applied to this mode. A candidate for $p \rightarrow e^+\omega (3\pi)$ was found in the SK-I data.

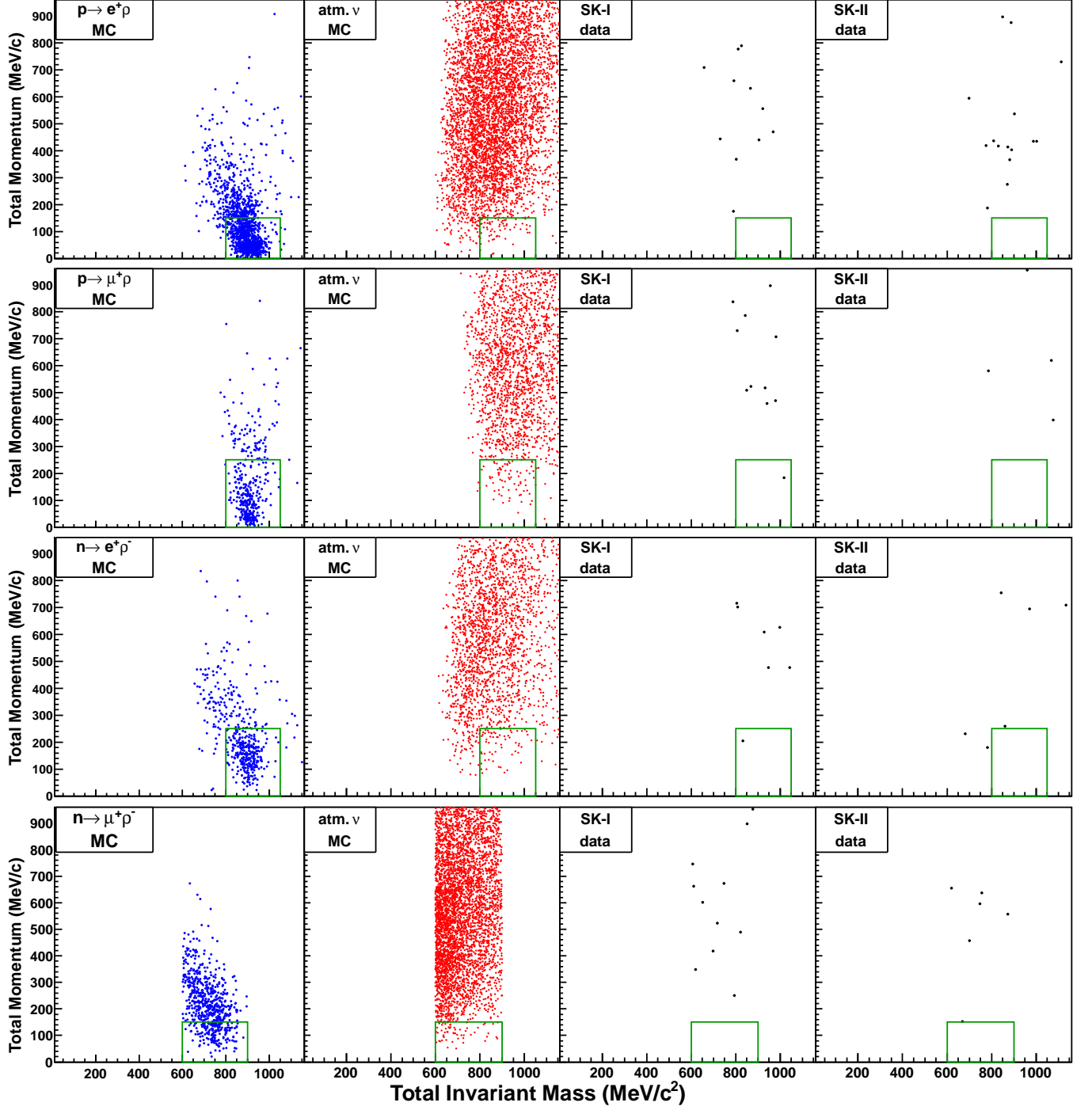


FIG. 14. Total momentum versus total invariant mass distributions of proton decay MC (SK-I+II combined), the atmospheric neutrino MC (SK-I+II combined; 11.25 megaton-years for each SK-I and SK-II) and SK-I (91.7 kiloton-years) and SK-II (49.2 kiloton-years) data, from top to bottom: $p \rightarrow e^+ \rho^0$, $p \rightarrow \mu^+ \rho^0$, $n \rightarrow e^+ \rho^-$ and $n \rightarrow \mu^+ \rho^-$. These events satisfy the event selection criteria for each mode except for the selection on total momentum and total mass. The boxes in figures indicate the total momentum and mass criteria. For the $n \rightarrow \mu^+ \rho^-$ mode, no total invariant mass cut is applied and the sharp cutoffs on the total invariant mass correspond to the ρ^- invariant mass cut threshold. A candidate for each $p \rightarrow \mu^+ \rho^0$ and $n \rightarrow e^+ \rho^-$ was found in the SK-I data.

For the total invariant mass reconstruction in the $n \rightarrow \mu^+\pi^-$ mode, it is necessary to determine which ring was made by the muon or the charged pion. As described before, the ring combination which falls closest to the neutron mass was selected. This resulted in a narrower invariant mass distribution for $n \rightarrow \mu^+\pi^-$ than that for the $n \rightarrow e^+\pi^-$ MC, as shown in Fig. 15.

B. Search Results in the SK-I and SK-II data

The result of the nucleon decay searches are summarized in Table IV. The detection efficiencies, expected backgrounds and number of candidate events are shown in the table. The number of events and detection efficiencies at each event selection step are shown in Fig. 6 for the three typical nucleon decay mode searches. Figure 6 shows the consistency between the observed data and the atmospheric neutrino background in terms of the number of events.

Because of the difficulty in detecting charged pions in a large water Cherenkov detector, the efficiencies for modes with charged pions are relatively lower. For the modes with only Cherenkov rings from a charged lepton (e or μ) and γ , high efficiencies were achieved. The highest efficiency mode is $p \rightarrow e^+\pi^0$. Its efficiency is 87% for free proton decay events. Also, the efficiencies for the SK-I free proton decay events in $p \rightarrow e^+\eta$ (2γ), $p \rightarrow e^+\eta$ ($3\pi^0$) and $p \rightarrow e^+\omega$ ($\pi^0\gamma$) are 74%, 67% and 83%, respectively. Nevertheless, the total efficiencies for these modes are much lower than $p \rightarrow e^+\pi^0$ due to the lower branching ratios for the meson decay modes.

The detection efficiencies in SK-II are lower than in SK-I. However, the difference is a only few percent for the modes with high detection efficiencies ($p \rightarrow e^+\pi^0$, $p \rightarrow e^+\eta$, etc.) and less than about 17% even for the modes with low efficiencies as shown in Table IV. Therefore, nucleon decay searches using SK-II data are comparable to those using SK-I data. The estimated background rates of SK-I and SK-II are also comparable to each other.

Charged current pion production from neutrino interactions was the dominant background source for most of the studied nucleon decay modes. The breakdown of background events is shown in Table V. Pions produced by neutrino interactions and/or hadronic interactions in nuclei and/or in water can mimic the event signatures of nucleon decay signals with a charged lepton. There was also a considerable contribution for the $p \rightarrow l^+\pi^0$ mode background from charged current quasi-elastic scattering (CCQE). A typical background event from CCQE is shown in Fig. 16. This is because a highly energetic proton (> 1 GeV/ c) produced by the interaction and scattered in water produces a secondary pion. Backgrounds of high ring multiplicity modes (four-ring or five-ring events) such as $p \rightarrow l^+\eta(3\pi)$ or $p \rightarrow l^+\omega(3\pi)$ have relatively higher fractions of multi-pion production events and has less dependency on whether the interaction is charged current or neutral current.

The consistency of the neutrino interactions and the nuclear effects was checked by comparing background estimations between our MC and NUANCE [38]. NUANCE has different models of neutrino interactions and nuclear effects. The atmospheric neutrino MC generated with NUANCE used the same atmospheric neutrino flux equivalent to 100 years (2.25 megaton-years exposure) and the same detector simulation. The results of these two estimates are also shown in Table IV. Estimates obtained with NUANCE MC were consistent with results from our MC in most of the modes.

In total, six candidate events were found in the SK-I and SK-II data in the modes; $p \rightarrow \mu^+\eta$ ($3\pi^0$), $p \rightarrow \mu^+\rho^0$, $p \rightarrow e^+\omega$ (3π), $n \rightarrow \mu^+\pi^-$ and $n \rightarrow e^+\rho^-$. As can be seen from Figures 11, 13, 14, 15, every candidate event was around the threshold of the selection window of total momentum and total invariant mass cut. A candidate event for $p \rightarrow e^+\omega$ (3π) (Fig. 17) has a vertex around the center of the detector and the smallest total momentum of all candidates, although there might be a PID misidentification for this event, which is described in the caption of the figure.

These candidates were found in the five modes. For the $p \rightarrow \mu^+\eta$ ($3\pi^0$) mode, there were two candidate events. The probability of observing more than two events from the expected background was calculated without systematic errors to be 7.5%. For the other modes with a candidate event, probabilities to observe one candidate from the expectations are about 30% for each. Because the probabilities for observing one (two) or more background events in our sample are not so small for the 16 decay modes, we cannot take the candidates as serious evidence of nucleon decay. Moreover, the number of background events in total was 4.7 events. Consequently, the number of candidates is consistent with the estimation by the atmospheric neutrino MC. Therefore, nucleon partial lifetime limits were calculated in Section VID.

C. Systematic Errors

Systematic errors for detection efficiencies and background estimations are described in this section. As for the exposure, the systematic errors of detector size and livetime are less than 1% and negligible.

1. Systematic Errors of Detection Efficiency

a. Nuclear Effect In most of the modes, meson (π , η , ω) nuclear effects (meson-nucleon interactions in a nucleus) have large effects on detection efficiencies and can be a dominant error source.

b. π nuclear effect The systematic uncertainties of π nuclear effects were estimated by comparing the nuclear effect simulation with another simulation result based on the model used by the IMB experiment [39] because there are no suitable experimental data which can be used for

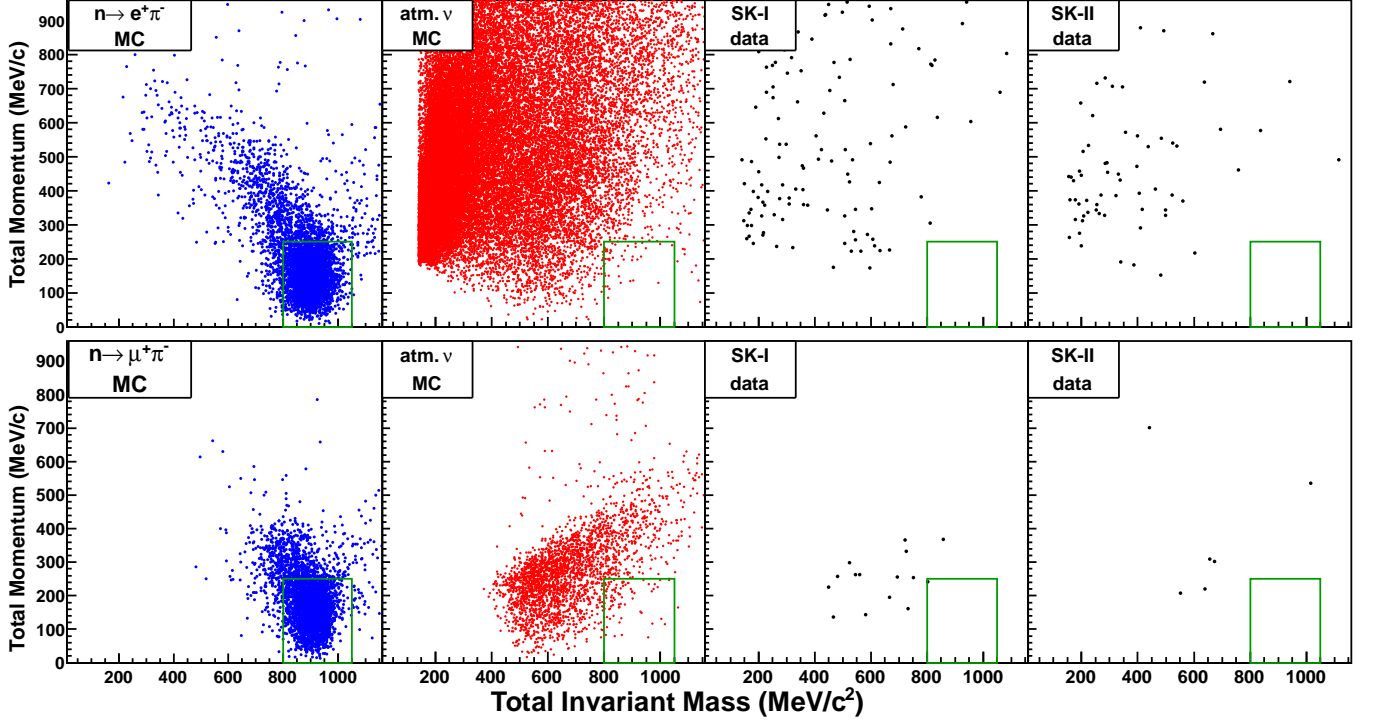


FIG. 15. Total momentum versus total invariant mass distributions of proton decay MC (SK-I+II combined), the atmospheric neutrino MC (SK-I+II combined; 11.25 megaton-years for each SK-I and SK-II) and SK-I (91.7 kiloton-years) and SK-II (49.2 kiloton-years) data, for $n \rightarrow e^+ \pi^-$ (top) and $n \rightarrow \mu^+ \pi^-$ (bottom). These events satisfy the event selection criteria for each mode except for the selection on the total momentum and total mass. The boxes in the figures indicate the total momentum and mass criteria. A candidate for $n \rightarrow \mu^+ \pi^-$ was found in the SK-I data.

Modes	Eff.(%)		Background			Candidate		Lifetime Limit ($\times 10^{33}$ years) at 90% CL
	SK-I	SK-II	SK-I	NEUT SK-II	NUANCE SK-I+II	SK-I	SK-II	
$p \rightarrow e^+ \pi^0$	44.6	43.5	0.20 ± 0.04 (2.1)	0.11 ± 0.02 (2.2)	0.27 ± 0.10	0	0	8.2
$p \rightarrow \mu^+ \pi^0$	35.5	34.7	0.23 ± 0.04 (2.5)	0.11 ± 0.02 (2.2)	0.27 ± 0.09	0	0	6.6
$p \rightarrow e^+ \eta$								4.2
($\eta \rightarrow 2\gamma$)	18.8	18.2	0.19 ± 0.04 (2.1)	0.09 ± 0.02 (1.8)	0.29 ± 0.10	0	0	
($\eta \rightarrow 3\pi^0$)	8.1	7.6	0.08 ± 0.03 (0.9)	0.08 ± 0.02 (1.7)	0.32 ± 0.11	0	0	
$p \rightarrow \mu^+ \eta$								1.3
($\eta \rightarrow 2\gamma$)	12.4	11.7	0.03 ± 0.02 (0.3)	0.01 ± 0.01 (0.2)	0.04 ± 0.04	0	0	
($\eta \rightarrow 3\pi^0$)	6.1	5.4	0.30 ± 0.05 (3.3)	0.15 ± 0.03 (2.9)	0.44 ± 0.13	0	2	
$p \rightarrow e^+ \rho^0$	4.9	4.2	0.23 ± 0.05 (2.5)	0.12 ± 0.02 (2.4)	0.34 ± 0.11	0	0	0.71
$p \rightarrow \mu^+ \rho^0$	1.8	1.5	0.30 ± 0.05 (3.3)	0.12 ± 0.02 (2.5)	0.46 ± 0.12	1	0	0.16
$p \rightarrow e^+ \omega$								0.32
($\omega \rightarrow \pi^0 \gamma$)	2.4	2.2	0.10 ± 0.03 (1.1)	0.04 ± 0.01 (0.9)	0.29 ± 0.10	0	0	
($\omega \rightarrow 3\pi$)	2.5	2.3	0.26 ± 0.05 (2.9)	0.13 ± 0.02 (2.6)	0.30 ± 0.11	1	0	
$p \rightarrow \mu^+ \omega$								0.78
($\omega \rightarrow \pi^0 \gamma$)	2.8	2.8	0.24 ± 0.05 (2.6)	0.07 ± 0.02 (1.4)	0.37 ± 0.11	0	0	
($\omega \rightarrow 3\pi$)	2.7	2.4	0.10 ± 0.03 (1.1)	0.07 ± 0.02 (1.3)	0.05 ± 0.04	0	0	
$n \rightarrow e^+ \pi^-$	19.4	19.3	0.16 ± 0.04 (1.7)	0.11 ± 0.02 (2.2)	0.37 ± 0.12	0	0	2.0
$n \rightarrow \mu^+ \pi^-$	16.7	15.6	0.30 ± 0.05 (3.3)	0.13 ± 0.02 (2.6)	0.44 ± 0.12	1	0	1.0
$n \rightarrow e^+ \rho^-$	1.8	1.6	0.25 ± 0.05 (2.7)	0.13 ± 0.02 (2.7)	0.44 ± 0.12	1	0	0.070
$n \rightarrow \mu^+ \rho^-$	1.1	0.94	0.19 ± 0.04 (2.1)	0.10 ± 0.02 (1.9)	0.69 ± 0.14	0	0	0.036

TABLE IV. Summary of the nucleon decay searches. Numbers in parentheses in backgrounds are exposure-normalized background rates in (megaton-years)⁻¹. Background errors shown here are statistical errors of finite MC statistics.

Mode	$p \rightarrow e^+\pi^0$	$N \rightarrow l^+\pi$	$p \rightarrow l^+\eta$	$p \rightarrow l^+\omega$	$N \rightarrow l^+\rho$
CCQE	28%	21%	5%	4%	9%
CC 1- π	32%	51%	20%	25%	45%
CC multi- π	19%	14%	24%	29%	14%
CC others	2%	6%	13%	7%	4%
NC	19%	9%	37%	35%	28%

TABLE V. The breakdown of the neutrino interaction modes of the background events. The breakdowns are calculated by simply adding background events of the modes decaying into each meson except for that of $p \rightarrow e^+\pi^0$.

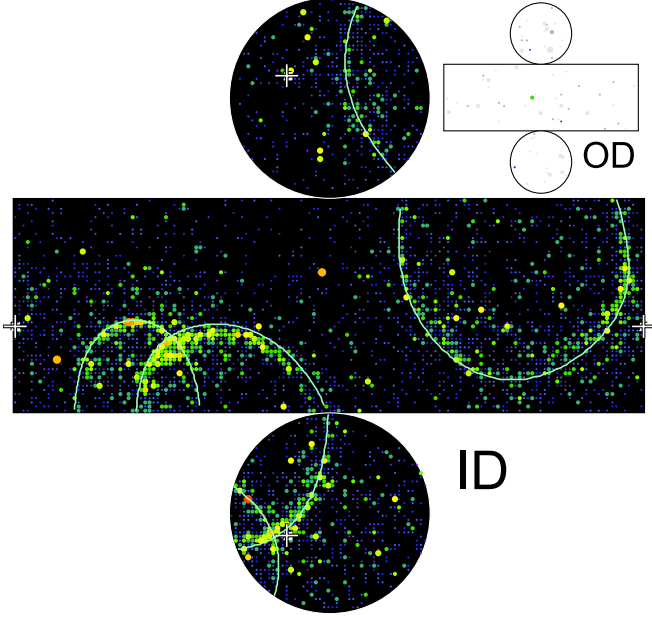


FIG. 16. An example of a background event for the $p \rightarrow e^+\pi^0$ mode in the atmospheric neutrino MC. An electron neutrino interacts with a neutron by CCQE and produces an electron and a proton. One ring from the electron and the other two rings from the decay of a π^0 , which is produced by a secondary interaction of the proton in water, mimic a proton decay signal from $p \rightarrow e^+\pi^0$. Solid line circles show reconstructed rings.

the systematic error estimation with enough precision at the moment. The comparison of the fraction of final states for the proton decay of $p \rightarrow e^+\pi^0$ in ^{16}O nuclei is shown in Table VI. The detection efficiency directly depends on the probability of the π^0 escaping without any scattering. There is a 10% difference in that probability between the two models. This difference corresponds to a 15% difference in the total detection efficiencies of $p \rightarrow e^+\pi^0$ and $p \rightarrow \mu^+\pi^0$.

The escape probability difference described above for the $p \rightarrow e^+\pi^0$ mode is equivalent to $\sim 40\%$ difference in the total cross-section of the π nuclear effect. Thus, this difference in the total cross-section was used for the systematic error estimates from π nuclear effects for the other nucleon decay modes, since detailed results of the

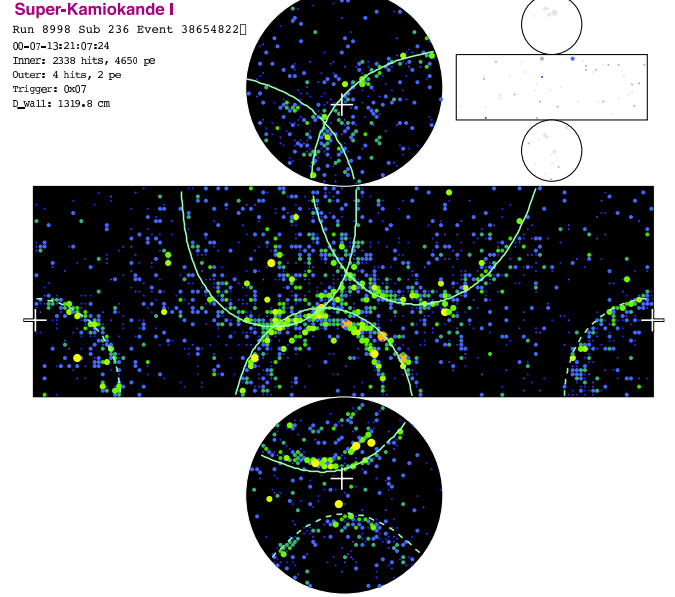


FIG. 17. A candidate event for $p \rightarrow e^+\omega$ (3π) in the SK-I data. Reconstructed total momentum and invariant mass were $137 \text{ MeV}/c$ and $796 \text{ MeV}/c^2$, respectively. Solid (dashed) lines correspond to reconstructed rings classified as shower (non shower) type. A Cherenkov ring at the center-bottom of the display was classified as a shower-type ring in the PID algorithm, but its Cherenkov ring edge looks as sharp as a non shower-type ring.

nuclear effect	Our MC	IMB
no interaction	44%	54%
absorption	22%	22%
charge exchange	15%	10%
scattered	19%	14%

TABLE VI. Fraction of the final states of π^0 from the proton decay of $p \rightarrow e^+\pi^0$ in ^{16}O compared with the simulation used in the IMB experiment.

IMB simulation were not available for those modes. As for the $n \rightarrow e^+\pi^-$ mode, the effect on the π^- escape probability from a 40% uncertainty on the π nuclear effect was estimated by the nucleon decay simulation. This effect corresponds to a 20% difference in the total detection efficiency for $n \rightarrow e^+\pi^-$. It is greater than that for $p \rightarrow e^+\pi^0$ because there are no free (unbound) nucleon decay events for $n \rightarrow e^+\pi^-$.

c. η nuclear effect The systematic uncertainty of η nuclear effects was estimated in Section III A 2 by comparing the experimental η photoproduction cross-section with the simulated cross-section. The estimated error for the η -nucleon cross-section in ^{16}O nuclei was a factor of 2.

Table VII shows the effects of the systematic uncertainties of the cross-section on the fraction of η meson final

η nuclear effect	$p \rightarrow l^+ \eta$	$\sigma \times \frac{1}{2}$	$\sigma \times 2$
no interaction	56%	73%	43%
scattered	6%	4%	5%
no η survived	38%	23%	53%

TABLE VII. Fraction of the final states of η meson from the proton decay of $p \rightarrow l^+ \eta$ in ^{16}O .

states from a proton decay in ^{16}O . The events in which no η meson escapes from a nucleus hardly passed the selection criteria. The efficiency for the events in which the η meson was scattered in the nucleus was less than $\sim 1/4$ of the efficiency for the events without any interactions in a nucleus. Therefore, effects on the detection efficiency could be estimated almost entirely by the change of the escape probability with no interaction in a nucleus. The estimated errors corresponded to a $\sim 20\%$ error in total detection efficiencies for $p \rightarrow e^+ \eta$ and $p \rightarrow \mu^+ \eta$.

d. ω nuclear effect The systematic uncertainty of ω nuclear effects was a factor of 3, which was estimated by the comparison of the ω -nucleon cross-section for the theoretical calculation and the extracted data from the ω photoproduction experiment as described in Section III A 3.

ω nuclear effect in ^{16}O	$p \rightarrow e^+ \omega$ $\sigma \times 3$		$p \rightarrow \mu^+ \omega$ $\sigma \times 3$	
no interaction	19%	11%	17%	10%
scattered	2%	2%	1%	1%
decay in a nucleus	53%	35%	56%	37%
$\omega N \rightarrow N + \text{meson} (\neq \omega)$	26%	52%	25%	51%

TABLE VIII. Fraction of the final states of the ω meson from the proton decay of $p \rightarrow e^+ \omega$ or $p \rightarrow \mu^+ \omega$ in ^{16}O .

The effect of the factor of 3 uncertainty of the cross-section has a large effect on the fraction of ω meson final states from $p \rightarrow e^+ \omega$ and $p \rightarrow \mu^+ \omega$ in an ^{16}O nucleus, as shown in Table VIII. However, these effects correspond to only a $\sim 20\%$ error on the total detection efficiency, since the fraction of free proton decay events, which do not suffer from nuclear effects, in the total surviving events was $40 \sim 60\%$ for the $p \rightarrow e^+ \omega$ and $p \rightarrow \mu^+ \omega$ search.

e. Hadron Propagation in Water In some of the nucleon decay mode searches, Cherenkov rings from charged pions were required to be found. Charged pions strongly interact with nucleons in water. Thus, whether charged pion rings can be observed or not depends on their hadronic interactions in water.

The uncertainty of the charged pion hadronic interaction cross-section in water was considered to be 10% by comparing the detector simulation with experimental data [40, 41].

Only for the systematic errors on the background, the uncertainty of the pion production probability by high momentum ($> \sim 1$ GeV/c) hadrons was also considered.

This error of the production probability was conservatively set to 100%.

f. Fraction of N-N Correlated Decay As described in Section III A, 10% of nucleons in an ^{16}O nucleus are assumed to correlate with another nucleon. Such a decay is calculated as a three-body decay. The detection efficiency for this decay can be very low. The uncertainty for this fraction was conservatively set to 100%.

g. Fermi Motion The total momentum of a bound nucleon decay event corresponds to the Fermi motion of the source nucleon. The systematic error from the uncertainty of the Fermi motion was estimated by comparing the distributions used in the simulation with the Fermi gas model or by changing the momentum by $\pm 20\%$. If a tighter total momentum cut is used, the systematic error from the Fermi motion can be large.

h. Fiducial Volume The systematic errors from the fiducial volume were estimated by the difference in the number of events for reconstructed and true vertices of multi-ring events. The estimated errors were 3% and 2% for SK-I and SK-II, respectively. This error can directly affect the detection efficiencies, but its magnitude is negligible compared with other systematic errors.

i. Momentum Scale The uncertainty of the momentum scale was estimated to be 1.1% (1.7%) in SK-I (SK-II) by the quadratic sum of the uncertainties of the absolute momentum scale and the time variation described in Section V B. The momentum scale non-uniformity in the detector was within $\pm 0.6\%$. The non-uniformity can cause momentum imbalance of an event, leading to a 1.2% error for the total momentum.

The systematic errors on the efficiencies were estimated by the changing the threshold of the momentum and mass in the selection criteria. These two errors have negligible effects.

j. PID, Ring Counting and Cherenkov Opening Angle The systematic error of the particle identification was estimated by comparing the likelihood difference (non shower-type likelihood - shower-type likelihood) distributions of observed data and atmospheric neutrino MC. The ring counting systematic error was also estimated by the same method. Those likelihood difference distributions of the data and MC agree well with each other, and systematic errors from the PID and the ring counting were estimated to be negligible.

As for the Cherenkov opening angle, the systematic error of the Cherenkov opening angle was estimated to be 0.7 (0.5) degrees in SK-I (SK-II) by comparing the opening angle distributions of the observed data and atmospheric neutrino MC for non-primary (not most energetic) non shower-type rings in fully contained sub-GeV events (in which visible energy is below 1.33 GeV). Charged pion momentum reconstruction largely depends on the opening angle. Thus, the systematic errors for the modes which need to reconstruct the charged pion momenta can be relatively large.

k. Vertex Shift The vertex position was reconstructed at the beginning of the event reconstruction.

The reconstructed vertex can affect all of the following reconstruction algorithms like the ring counting, the PID, the momentum determination, etc.

The systematic error from the uncertainty of the vertex position was estimated by shifting the reconstructed vertex by 30 cm along the direction of the most energetic particle momentum. This was a conservative estimate since the systematic shift on that direction could cause largest error on the other event reconstructions. The shift length 30 cm corresponds to the typical resolution scale for the nucleon decay events as well as the scale of the uncertainty of the vertex position estimated by comparing different vertex fitting algorithms.

l. Summary of the Systematic Errors of Detection Efficiencies Table IX summarizes the results of the systematic error estimation for detection efficiencies of all modes. The systematic errors for detection efficiencies were about 20 ~ 30% except for the much large error of the $n \rightarrow l^+ \rho^-$ mode.

Systematic uncertainties of nuclear effects are the dominant error sources for most of the modes. For the $n \rightarrow e^+ \rho^-$ and $n \rightarrow \mu^+ \rho^-$ modes, the systematic errors from the pion nuclear effects are very large because both of the pions from the ρ meson decay were required to escape from the nucleus. Positive and negative errors were individually estimated especially for these two modes. On the other hand, $p \rightarrow e^+ \rho^0$ and $p \rightarrow \mu^+ \rho^0$ has a comparably smaller error since most of the surviving events in these modes are free proton decay events. The uncertainty of Fermi motion can be a dominant error source especially in modes using a tight total momentum cut like $p \rightarrow e^+ \eta$ ($3\pi^0$). Another important error is the reconstruction biases from the Cherenkov opening angle reconstruction and the vertex shift. These biases mostly contribute errors for the modes which require charged pion momentum reconstruction.

These dominant errors are mostly common in SK-I and SK-II. There are no significant differences between the systematic errors of SK-I and SK-II.

2. Systematic Errors of Background Estimation

For the background estimations from atmospheric neutrinos, the uncertainties of atmospheric neutrino flux and neutrino cross-sections were considered. The systematic uncertainties of pion nuclear effects, hadron propagation in water and the detector performance were also considered as well as the detection efficiencies.

Even with the large statistics of the atmospheric neutrino MC, only a few tens of events can survive the nucleon decay event selection criteria. In order to reduce statistical errors for the systematic error estimation of the background, systematic errors were estimated by averaging the estimations of SK-I and SK-II because they were basically common as described in the error estimation for the detection efficiencies. Moreover, for the modes with the same meson decay modes, systematic errors from the

uncertainties of pion nuclear effects and hadron interactions in water were estimated by averaging the estimations of different charged lepton modes.

Almost the same systematic uncertainties as the atmospheric neutrino oscillation analysis in the Super-Kamiokande experiment were considered for the errors from the neutrino flux and the neutrino interaction. The details of the source of the uncertainties are given in [36, 42]. The systematic errors from the neutrino flux were estimated to be 6 ~ 8%, and mostly due to the uncertainty of the energy spectrum. These errors are negligible compared with the other much larger errors. The systematic errors from the neutrino interactions were also estimated to be negligible, 8 ~ 16 %.

The estimated systematic errors for the backgrounds are shown in Table X. The systematic errors for the backgrounds ranged from about 40 to 70%. One of the dominant errors comes from the uncertainty of the pion-nucleon cross-section and the pion production probability in water. The errors from the detector and event reconstruction performances also have non-negligible contributions. The number of background events is very sensitive to the error of energy and momentum, since surviving background events are usually distributed around the threshold of the selection window of momentum and invariant mass. Therefore, the systematic error from the energy scale stability, which was negligible for the detection efficiencies, was estimated to be about 10 ~ 20%. The systematic shift of the reconstructed vertex can cause errors in the Cherenkov opening angle and opening angles between two particles, which are important for momentum and mass reconstruction. For the same reason as energy scale, the systematic error from the vertex shift was larger than that for the detection efficiency, and estimated to be about 10 ~ 50%.

D. Lifetime Limit

The observed data in SK-I and SK-II are consistent with the atmospheric neutrino MC. Consequently, lower limits on the nucleon partial lifetime were calculated.

The partial lifetime limit for each mode is derived from Bayes' theorem which incorporates systematic errors. Because the nucleon decay search is a counting experiment, the probability to detect n events is given by Poisson statistics as follows.

$$\mathbf{P}(n|\Gamma\lambda\epsilon b) = \frac{e^{-(\Gamma\lambda\epsilon+b)} (\Gamma\lambda\epsilon+b)^n}{n!} \quad (6)$$

where Γ is the true decay rate, λ is the true exposure, ϵ is the true detection efficiency, b is the true number of background events, and $\mathbf{P}(A|B)$ is the conditional probability of A, given that proposition B is true.

Applying Bayes' theorem allows us to write:

$$\mathbf{P}(\Gamma\lambda\epsilon b|n) = \frac{1}{A} \mathbf{P}(n|\Gamma\lambda\epsilon b) \mathbf{P}(\Gamma\lambda\epsilon b) \quad (7)$$

Mode	meson nuclear effect	hadron propagation in water	$N-N$ correlated decay	Fermi momentum	Detector Performances	Total
$p \rightarrow e^+\pi^0$	15%	-	7%	8%	4%	19%
$p \rightarrow \mu^+\pi^0$	15%	-	7%	8%	4%	19%
$p \rightarrow e^+\eta (2\gamma)$	20%	-	7%	13%	5%	25%
$p \rightarrow \mu^+\eta (2\gamma)$	18%	-	7%	14%	4%	24%
$p \rightarrow e^+\eta (3\pi^0)$	15%	-	5%	26%	9%	32%
$p \rightarrow \mu^+\eta (3\pi^0)$	20%	-	7%	14%	10%	28%
$p \rightarrow e^+\rho^0$	8%	17%	2%	10%	18%	28%
$p \rightarrow \mu^+\rho^0$	9%	24%	2%	6%	11%	29%
$p \rightarrow e^+\omega (\pi^0\gamma)$	21%	-	5%	24%	9%	33%
$p \rightarrow \mu^+\omega (\pi^0\gamma)$	23%	-	6%	13%	7%	28%
$p \rightarrow e^+\omega (\pi^+\pi^-\pi^0)$	19%	13%	5%	12%	20%	34%
$p \rightarrow \mu^+\omega (\pi^+\pi^-\pi^0)$	19%	15%	5%	2%	16%	29%
$n \rightarrow e^+\pi^-$	20%	9%	11%	12%	12%	30%
$n \rightarrow \mu^+\pi^-$	24%	6%	11%	7%	17%	33%
$n \rightarrow e^+\rho^-$	+51% -23%	9%	11%	15%	19%	+59% -37%
$n \rightarrow \mu^+\rho^-$	+51% -25%	14%	10%	27%	23%	+65% -47%

TABLE IX. Systematic errors for detection efficiencies. The errors of SK-I and SK-II were separately estimated and averaged by the livetime.

Mode	neutrino flux	neutrino cross section	pion nuclear effect	hadron propagation in water	Detector Performances	Total
$p \rightarrow e^+\pi^0$	8%	8%	8%	36%	22%	44%
$p \rightarrow \mu^+\pi^0$	8%	8%	8%	36%	43%	58%
$p \rightarrow e^+\eta (2\gamma)$	8%	11%	5%	36%	26%	47%
$p \rightarrow \mu^+\eta (2\gamma)$	8%	14%	5%	36%	28%	49%
$p \rightarrow e^+\eta (3\pi^0)$	8%	15%	18%	67%	13%	76%
$p \rightarrow \mu^+\eta (3\pi^0)$	8%	11%	18%	67%	20%	73%
$p \rightarrow e^+\rho^0$	6%	13%	14%	33%	33%	51%
$p \rightarrow \mu^+\rho^0$	8%	15%	14%	33%	23%	46%
$p \rightarrow e^+\omega (\pi^0\gamma)$	8%	14%	13%	41%	37%	59%
$p \rightarrow \mu^+\omega (\pi^0\gamma)$	8%	10%	13%	41%	28%	53%
$p \rightarrow e^+\omega (\pi^+\pi^-\pi^0)$	7%	14%	8%	53%	28%	63%
$p \rightarrow \mu^+\omega (\pi^+\pi^-\pi^0)$	7%	11%	8%	53%	29%	63%
$n \rightarrow e^+\pi^-$	8%	15%	8%	36%	46%	61%
$n \rightarrow \mu^+\pi^-$	8%	16%	8%	36%	36%	55%
$n \rightarrow e^+\rho^-$	8%	14%	12%	18%	54%	60%
$n \rightarrow \mu^+\rho^-$	6%	16%	12%	18%	27%	39%

TABLE X. Systematic errors for background estimates.

where A is the constant to normalize $\mathbf{P}(\Gamma\lambda\epsilon b|n)$. Because the decay rate, the detection efficiency, the exposure and the background are independent, $\mathbf{P}(\Gamma\lambda\epsilon b)$ can be separated into constituents.

$$\mathbf{P}(\Gamma\lambda\epsilon b|n) = \frac{1}{A}\mathbf{P}(n|\Gamma\lambda\epsilon b)\mathbf{P}(\Gamma)\mathbf{P}(\epsilon)\mathbf{P}(\lambda)\mathbf{P}(b) \quad (8)$$

The probability density function of Γ can be defined

as;

$$\begin{aligned} \mathbf{P}(\Gamma|n) &= \int \int \int \mathbf{P}(\Gamma\lambda\epsilon b|n)d\epsilon d\lambda db \\ &= \frac{1}{A} \int \int \int \frac{e^{-(\Gamma\lambda\epsilon+b)} (\Gamma\lambda\epsilon+b)^n}{n!} \\ &\quad \times \mathbf{P}(\Gamma)\mathbf{P}(\epsilon)\mathbf{P}(\lambda)\mathbf{P}(b)d\epsilon d\lambda db \end{aligned} \quad (9)$$

where $\mathbf{P}(\Gamma)$, $\mathbf{P}(\lambda)$, $\mathbf{P}(\epsilon)$ and $\mathbf{P}(b)$ are the prior probability distributions, in which systematic uncertainties can be incorporated.

The priors for the exposure, the detection efficiency and the background are assumed to be truncated Gaus-

sian distributions defined as;

$$\mathbf{P}(x) \propto \begin{cases} \exp\left(-\frac{(x-x_0)^2}{2\sigma_x^2}\right) & (x > 0) \\ 0 & (x \leq 0) \end{cases} \quad (10)$$

$(x = \lambda, \epsilon, b)$

where λ_0 (σ_λ), ϵ_0 (σ_ϵ) and b (σ_b) are the estimates (systematic errors) of the detection efficiency, the exposure and the background, respectively. If the systematic error for the detection efficiency is assumed to be asymmetric, the prior $\mathbf{P}(\epsilon)$ is an asymmetric Gaussian.

The prior for the decay rate is assumed to be uniform. This is implicitly assumed when calculating limits by simple Poisson statistics without systematic errors.

$$\mathbf{P}(\Gamma) = \begin{cases} 1 & (0 < \Gamma < \Gamma_{\text{cut}}) \\ 0 & (\Gamma \leq 0 \text{ or } \Gamma \geq \Gamma_{\text{cut}}) \end{cases} \quad (11)$$

where Γ_{cut} is the upper limit of the decay rate for the calculation of the normalization constant A in order to avoid divergence. The upper limit Γ_{cut} is set to be 10^{-31} years $^{-1}$, which is sufficiently larger than the limits by the previous experiments.

By integrating Equation (9) using the priors, the confidence level can be calculated as;

$$CL = \int_0^{\Gamma_{\text{limit}}} \mathbf{P}(\Gamma|n)d\Gamma. \quad (12)$$

Lifetime limits are obtained by:

$$\tau_{\text{limit}} = 1/\Gamma_{\text{limit}}. \quad (13)$$

The combined result of SK-I and SK-II is also derived by the method described above. The probability to detect n_1 events in SK-I and n_2 events in SK-II is the product of the two Poisson probabilities.

$$\mathbf{P}(n_1, n_2 | \Gamma \lambda_1 \epsilon_1 b_1 \lambda_2 \epsilon_2 b_2) = \mathbf{P}(n_1 | \Gamma \lambda_1 \epsilon_1 b_1) \mathbf{P}(n_2 | \Gamma \lambda_2 \epsilon_2 b_2) \quad (14)$$

We apply Bayes' theorem assuming that the decay rate, the exposure, the detection efficiency and the background are independent:

$$\mathbf{P}(\Gamma \lambda_1 \epsilon_1 b_1 \lambda_2 \epsilon_2 b_2 | n_1, n_2) = \frac{1}{A} \mathbf{P}(n_1, n_2 | \Gamma \lambda_1 \epsilon_1 b_1 \lambda_2 \epsilon_2 b_2) \times \mathbf{P}(\Gamma) \mathbf{P}(\epsilon_1, \epsilon_2) \mathbf{P}(\lambda_1, \lambda_2) \mathbf{P}(b_1, b_2). \quad (15)$$

Most of the dominant systematic uncertainties like the nuclear effects and hadron propagation in water are common between SK-I and SK-II. Therefore, the systematic errors of SK-I and SK-II are assumed to be fully correlated with each other, which gives conservative lifetime limits for this method. Then, the priors for the exposure, the detection efficiency and the background of SK-I and SK-II are expressed as:

$$\mathbf{P}(x_1, x_2) = \mathbf{P}(\delta_x) \propto \exp\left(-\frac{\delta_x^2}{2}\right) \quad (16)$$

$(x = \lambda, \epsilon, b)$

where δ_x is a correlated error factor for SK-I and SK-II defined as follows:

$$\delta_x = \frac{(x_1 - x_{01})}{\sigma_{x1}} = \frac{(x_2 - x_{02})}{\sigma_{x2}} \quad (17)$$

$(x = \lambda, \epsilon, b)$

λ_{0i} , ϵ_{0i} and b_{0i} are the estimated exposure, detection efficiency and background for SK-I and SK-II, respectively. The statistical error of the background MC is ignored because of the much larger systematic errors.

Finally the probability density function can be expressed as:

$$\mathbf{P}(\Gamma | n_1, n_2) = \frac{1}{A} \int \int \int \frac{e^{-(\Gamma \lambda_1 \epsilon_1 + b_1)} (\Gamma \lambda_1 \epsilon_1 + b_1)^{n_1}}{n_1!} \times \frac{e^{-(\Gamma \lambda_2 \epsilon_2 + b_2)} (\Gamma \lambda_2 \epsilon_2 + b_2)^{n_2}}{n_2!} \times \mathbf{P}(\Gamma) \mathbf{P}(\delta_\epsilon) \mathbf{P}(\delta_\lambda) \mathbf{P}(\delta_b) d\delta_\epsilon d\delta_\lambda d\delta_b. \quad (18)$$

The confidence level and lifetime limit are calculated by integrating this probability density function as in Equations 12 and 13.

For a mode with two different meson decay modes like $\eta \rightarrow 2\gamma$ and $\eta \rightarrow 3\pi^0$, the efficiencies and the backgrounds were simply added because such different meson decay mode searches are independent. The systematic errors on the detection efficiencies and the backgrounds were also simply added assuming 100% correlation.

The nucleon partial lifetime limits at 90% confidence level were obtained and summarized in Table IV and also shown in Fig. 18.

VII. CONCLUSION

Nucleon decays into a charged anti-lepton (e^+ and μ^+) plus a light meson (π^0 , π^- , η , ρ^0 , ρ^- and ω) were searched for in 91.7 and 49.2 kiloton-year exposures of the SK-I and SK-II data, respectively.

Performances for nucleon decay searches were compared between SK-I and SK-II. The observation in the SK-II period had similar performance to that in the SK-I period even though the photocathode coverage was half of SK-I.

No evidence for proton decays via the $p \rightarrow e^+\pi^0$ mode was found, though this mode has the highest detection efficiency and is the dominant proton decay mode in various GUT models. Six candidate events were found in the SK-I and SK-II data for the five largest-background modes. The total expected background from atmospheric neutrinos was 4.7 events. The number and features of candidate events are consistent with the background estimate by the atmospheric neutrino MC.

Nucleon partial lifetime limits were calculated based on Bayes' theorem. The lower limit on the partial lifetime of the proton via the $p \rightarrow e^+\pi^0$ mode was calculated to be 8.2×10^{33} years at 90% confidence level.

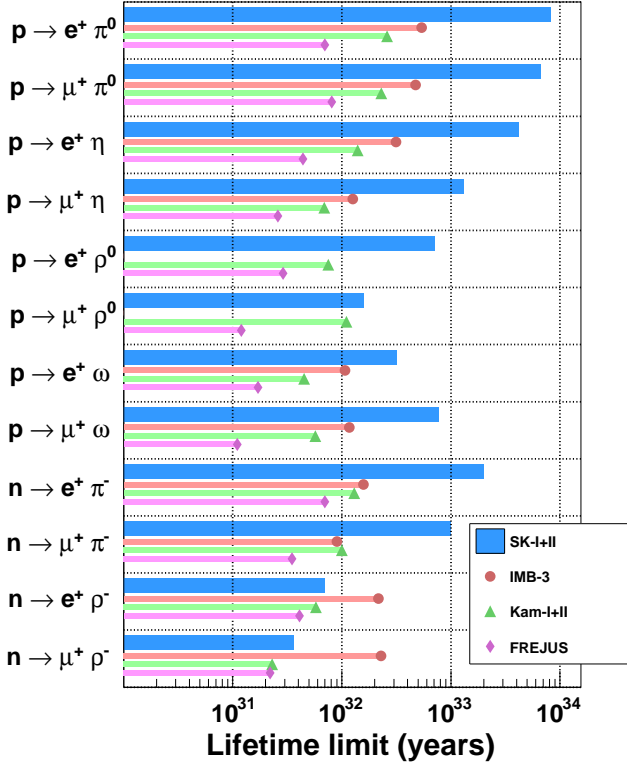


FIG. 18. Explored ranges and lower limits (at 90% confidence level) of nucleon partial lifetime with the results of the previous experiments; IMB-3 [4], KAMIOKANDE-I+II [5] and FREJUS [43].

As for the $p \rightarrow e^+\pi^0$ and $p \rightarrow \mu^+\pi^0$ modes, we have applied the same set of cuts to an increased exposure of the Super-Kamiokande detector and found no candidates. The new exposure includes running periods of SK-III and SK-IV. SK-III has restored photocoverage of 11100 PMTs, but with the acrylic shields introduced for SK-II. The SK-IV running includes new electronics. The same proton decay signal and atmospheric neutrino Monte Carlo methods were used to estimate the signal efficiency and background. We found for SK-III the efficiency for $p \rightarrow e^+\pi^0$ to be 45.2% and the efficiency for $p \rightarrow \mu^+\pi^0$ to be 36.3%, with background rates of 1.9 events/megaton-year and 2.5 events/megaton-year respectively. For SK-IV we found the efficiency for $p \rightarrow e^+\pi^0$ to be 45.0% and the efficiency for $p \rightarrow \mu^+\pi^0$ to be 43.9%, with background rates of 1.7 events/megaton-year and 3.6 events/megaton-year respectively. These numbers are consistent with the efficiencies and background rates presented in this paper, with the exception that the

increased efficiency for $p \rightarrow \mu^+\pi^0$ in SK-IV is attributed to an increased efficiency for muon-decay electron finding due to the improved electronics of SK-IV. The distributions of total invariant mass and total momentum are substantially similar to those for SK-I and SK-II presented in Fig. 10. As a result of finding no candidates, we also report an updated lifetime limit for 219.7 kt-years of SK-I, II, III, and IV exposure, finding $\tau/B > 1.29 \times 10^{34}$ years for $p \rightarrow e^+\pi^0$ and $\tau/B > 1.08 \times 10^{34}$ years for $p \rightarrow \mu^+\pi^0$ at 90% CL.

The obtained lower partial lifetime limits via the other modes except for $n \rightarrow e^+\rho^-$ and $n \rightarrow \mu^+\rho^-$ are also more stringent than the previous limits by IMB-3 or KAMIOKANDE-I+II. They range from 1.6×10^{32} to 6.6×10^{33} years. The obtained lifetime limits for the $n \rightarrow e^+\rho^-$ and $n \rightarrow \mu^+\rho^-$ modes are 7.0×10^{31} and 3.6×10^{31} years, respectively. They are less stringent than the IMB-3 result. For the case of the $n \rightarrow e^+\rho^-$ mode, the signal efficiency and estimated background in IMB-3 are 49% (without uncertainty) and 6.3×10^2 events/megaton-year, respectively, with the cuts optimized to obtain the best lifetime limit expectation. On the other hand, we applied tighter selection criteria to reduce the huge backgrounds to 2.7 events/megaton-year, resulting in a smaller signal efficiency with an assigned uncertainty of $1.7^{+1.0}_{-0.7}\%$. The smaller efficiency and determined uncertainty are the main reasons why the obtained limit is less stringent than IMB-3. The same applies to the $n \rightarrow \mu^+\rho^-$ mode.

This systematic study does not rule out specific GUT models, such as SUSY SU(5), SO(10) and so on, but can constrain parameters relevant to nucleon decay mediated by a super-heavy gauge boson.

ACKNOWLEDGMENTS

We gratefully acknowledge the cooperation of the Kamioka Mining and Smelting Company. The Super-Kamiokande experiment has been built and operated from funding by the Japanese Ministry of Education, Culture, Sports, Science and Technology, the United States Department of Energy, and the U.S. National Science Foundation. Some of us have been supported by funds from the Korean Research Foundation (BK21), the National Research Foundation of Korea (NRF-20110024009), the State Committee for Scientific Research in Poland (grant1757/B/H03/2008/35), the Japan Society for the Promotion of Science, and the National Natural Science Foundation of China under Grants No. 10575056.

[1] H. Georgi and S. L. Glashow, Phys. Rev. Lett. **32**, 438 (1974).

[2] P. Langacker, Phys. Rept. **72**, 185 (1981).

[3] P. Langacker, (1994), arXiv:hep-ph/9411247.

- [4] C. McGrew *et al.*, Phys. Rev. **D59**, 052004 (1999).
- [5] K. S. Hirata *et al.* (KAMIOKANDE-II), Phys. Lett. **B220**, 308 (1989).
- [6] J. C. Pati and A. Salam, Phys. Rev. **D10**, 275 (1974).
- [7] D. G. Lee, R. N. Mohapatra, M. K. Parida, and M. Rani, Phys. Rev. **D51**, 229 (1995), arXiv:hep-ph/9404238.
- [8] N. T. Shaban and W. J. Stirling, Phys. Lett. **B291**, 281 (1992).
- [9] J. C. Pati, Int. J. Mod. Phys. **A18**, 4135 (2003), arXiv:hep-ph/0305221.
- [10] H. D. Kim and S. Raby, JHEP **01**, 056 (2003), arXiv:hep-ph/0212348.
- [11] W. Buchmuller, L. Covi, D. Emmanuel-Costa, and S. Wiesenfeldt, JHEP **09**, 004 (2004), arXiv:hep-ph/0407070.
- [12] J. R. Ellis, D. V. Nanopoulos, and J. Walker, Phys. Lett. **B550**, 99 (2002), arXiv:hep-ph/0205336.
- [13] H. Nishino *et al.* (Super-Kamiokande), Phys. Rev. Lett. **102**, 141801 (2009), arXiv:0903.0676 [hep-ex].
- [14] J. L. Raaf *et al.*, Talk given at "Fundamental Physics at the Intensity Frontier" (Rockville, Maryland, USA, 2011).
- [15] M. Machacek, Nucl. Phys. **B159**, 37 (1979).
- [16] M. B. Gavela, A. Le Yaouanc, L. Oliver, O. Pene, and J. C. Raynal, Phys. Lett. **B98**, 51 (1981).
- [17] J. F. Donoghue, Phys. Lett. **B92**, 99 (1980).
- [18] F. Buccella, G. Miele, L. Rosa, P. Santorelli, and T. Tuzi, Phys. Lett. **B233**, 178 (1989).
- [19] V. S. Berezinsky, B. L. Ioffe, and Y. I. Kogan, Phys. Lett. **B105**, 33 (1981).
- [20] K. Kobayashi *et al.* (Super-Kamiokande), Phys. Rev. **D72**, 052007 (2005), arXiv:hep-ex/0502026.
- [21] Y. Fukuda *et al.*, Nucl. Instrum. Meth. **A501**, 418 (2003).
- [22] K. Nakamura *et al.*, Nucl. Phys. **A268**, 381 (1976).
- [23] T. Yamazaki and Y. Akaishi, Phys. Lett. **B453**, 1 (1999).
- [24] "Geant detector description and simulation tool," (1993), CERN Program Library Long Writeup W5013.
- [25] T. A. Gabriel, J. E. Brau, and B. L. Bishop, IEEE Trans. Nucl. Sci. **36**, 14 (1989).
- [26] M. Nakahata *et al.* (KAMIOKANDE), J. Phys. Soc. Jap. **55**, 3786 (1986).
- [27] L. L. Salcedo, E. Oset, M. J. Vicente-Vacas, and C. Garcia-Recio, Nucl. Phys. **A484**, 557 (1988).
- [28] G. Rowe, M. Salomon, and R. H. Landau, Phys. Rev. **C18**, 584 (1978).
- [29] M. Roebig-Landau *et al.*, Phys. Lett. **B373**, 45 (1996).
- [30] <http://gwdac.phys.gwu.edu>.
- [31] B. Krusche *et al.*, Phys. Lett. **B358**, 40 (1995).
- [32] G. I. Lykasov, W. Cassing, A. Sibirtsev, and M. V. Rzyanin, Eur. Phys. J. **A6**, 71 (1999), arXiv:nucl-th/9811019.
- [33] M. Kotulla *et al.* (CBELSA/TAPS), Phys. Rev. Lett. **100**, 192302 (2008), arXiv:0802.0989 [nucl-ex].
- [34] Y. Hayato, Nucl. Phys. B Proc. Suppl. **112**, 171 (2002).
- [35] M. Honda, T. Kajita, K. Kasahara, S. Midorikawa, and T. Sanuki, Phys. Rev. **D75**, 043006 (2007), arXiv:astro-ph/0611418.
- [36] Y. Ashie *et al.* (Super-Kamiokande), Phys. Rev. **D71**, 112005 (2005), arXiv:hep-ex/0501064.
- [37] S. Mine *et al.* (K2K), Phys. Rev. **D77**, 032003 (2008).
- [38] D. Casper, Nucl. Phys. Proc. Suppl. **112**, 161 (2002), arXiv:hep-ph/0208030.
- [39] H. W. Bertini, Phys. Rev. **C6**, 631 (1972).
- [40] C. H. Q. Ingram *et al.*, Phys. Rev. **C27**, 1578 (1983).
- [41] J. P. Albanese *et al.*, Nucl. Phys. **A350**, 301 (1980).
- [42] R. Wendell *et al.* (Super-Kamiokande), Phys. Rev. **D81**, 092004 (2010), arXiv:1002.3471 [hep-ex].
- [43] C. Berger *et al.* (Frejus), Z. Phys. **C50**, 385 (1991).